

N 70-29019

## Department of Electrical Engineering

THE APPLICATION OF SEMICONDUCTORS TO  
QUASI-OPTICAL ISOLATORS FOR USE  
AT SUBMILLIMETER WAVELENGTHS

by

M. Kanda  
G. Masclet  
W.G. May  
R.E. Hayes

UNIVERSITY OF COLORADO  
BOULDER, COLORADO



CASE FILE  
COPY

THE APPLICATION OF SEMICONDUCTORS TO  
QUASI-OPTICAL ISOLATORS FOR USE  
AT SUBMILLIMETER WAVELENGTHS

by

M. Kanda  
G. Masclet  
W.G. May  
R.E. Hayes

April 1970

Prepared under Grant No. NGL06-003-088 by

Electrical Engineering Department  
University of Colorado  
Boulder, Colorado

for

Electronics Research Center

National Aeronautics and Space Administration

## ABSTRACT

An experimental and theoretical investigation of the utilization of anisotropic effects in semiconductor plasmas for the development of submillimeter wavelength isolators is described. The topics reported or include an new type of isolator that depends on reflection from a semiconductor surface, and one which uses Faraday rotation in semiconductors. Experiments at 94GHz that verify the basic validity of the reflection isolator theory are reported. The theory of these devices predicts that room temperature operation at 118 microns, using InSb and a magnetic field of 16 kG, with a forward loss of much less than one db and a reverse loss of about 25 db is possible. The analytical study of Faraday rotation isolators also predicts forward losses of less than one db.

## TABLE OF CONTENTS

### ABSTRACT

1. Introduction
2. Nonreciprocal Reflection Beam Isolator
  - 2.1 Introduction
  - 2.2 Theoretical Derivation of Reflection Coefficient
  - 2.3 Experimental Procedure
  - 2.4 Experimental Results
    - 2.4.1 Measurement of GaAs and InSb Parameters
    - 2.4.2 Comparison of Experimental Results with Theory
  - 2.5 Conclusions and Future Plans
3. Far Infrared Isolators using Faraday Rotation
  - 3.1 Introduction
  - 3.2 Theory
  - 3.3 Device Applications
    - 3.3.1 Isolator
    - 3.3.2 Modulators
  - 3.4 Experimental Apparatus
  - 3.5 Conclusions and Future Plans

### APPENDIX A

### APPENDIX B

### REFERENCES

## 1. Introduction

The purpose of the work described in this report is to investigate the utilization of anisotropic effects in a semiconductor plasma for the development of submillimeter wavelength control devices such as isolators and circulators. The potential importance of nonreciprocal semiconductor devices is in the flexibility of design that comes with the wide range of semiconductor parameters that can be easily achieved, in the possible compatibility with other semiconductor devices, and also in the new geometrical configurations that result when the primary field that interacts with the material is the microwave electric field and not the microwave magnetic field as in the case of ferrites.

The work reported here is a continuation of that reported in a previous report titled The Application of Semiconductors To Quasi-Optical and Waveguide Isolators For Use At Millimeter Wavelengths, dated July, 1969.

The topics which have been investigated during the 6 month report period beginning June 1, 1969 include a new class of isolators that depend on the reflection of incident electromagnetic radiation from a semiconductor magneto-plasma. This work is discussed in Section 2. Also included, in Section 3, are the results obtained from the continuing study of quasi-optical isolators that depend on Faraday rotation in semiconductors.

## 2. Nonreciprocal Reflection Beam Isolator

### 2.1 Introduction

The phenomena of nonreciprocal reflection of an electromagnetic wave incident on a magneto-plasma have been studied theoretically and experimentally at microwave frequencies.

N.F. Barber and D.D. Crombie (1) found that when the angle of incidence is large, the reflection coefficient for em waves in the ionosphere incident from the west is numerically greater than that for waves incident from the east, as shown in Fig. 1. In this case the magnetic field is that of the earth and the reflecting medium is a layer of the gaseous plasma of the ionosphere. J.R. Wait (2) considered the interaction of electromagnetic waves and plasma and solved the boundary value problem for the wave propagation transverse to the magnetic field. When the magnetic field is not transverse to the direction of propagation, the formulation is a great deal more complicated. J.M. Seaman (3) performed the experiment at 300°K and 92 GHz using 1.65  $\Omega$ -cm n-type GaAs as the plasma medium. Non-reciprocity was observed when the incident electric field is polarized in the plane of incidence and propagates transversely to a static magnetic field which is parallel to the plasma surface. At an angle of incidence  $\theta$ , measured with respect to the surface normal, of 60° and a field of 13.2 kilogauss a forward loss of 11db and a reverse loss of 13.5db were obtained,



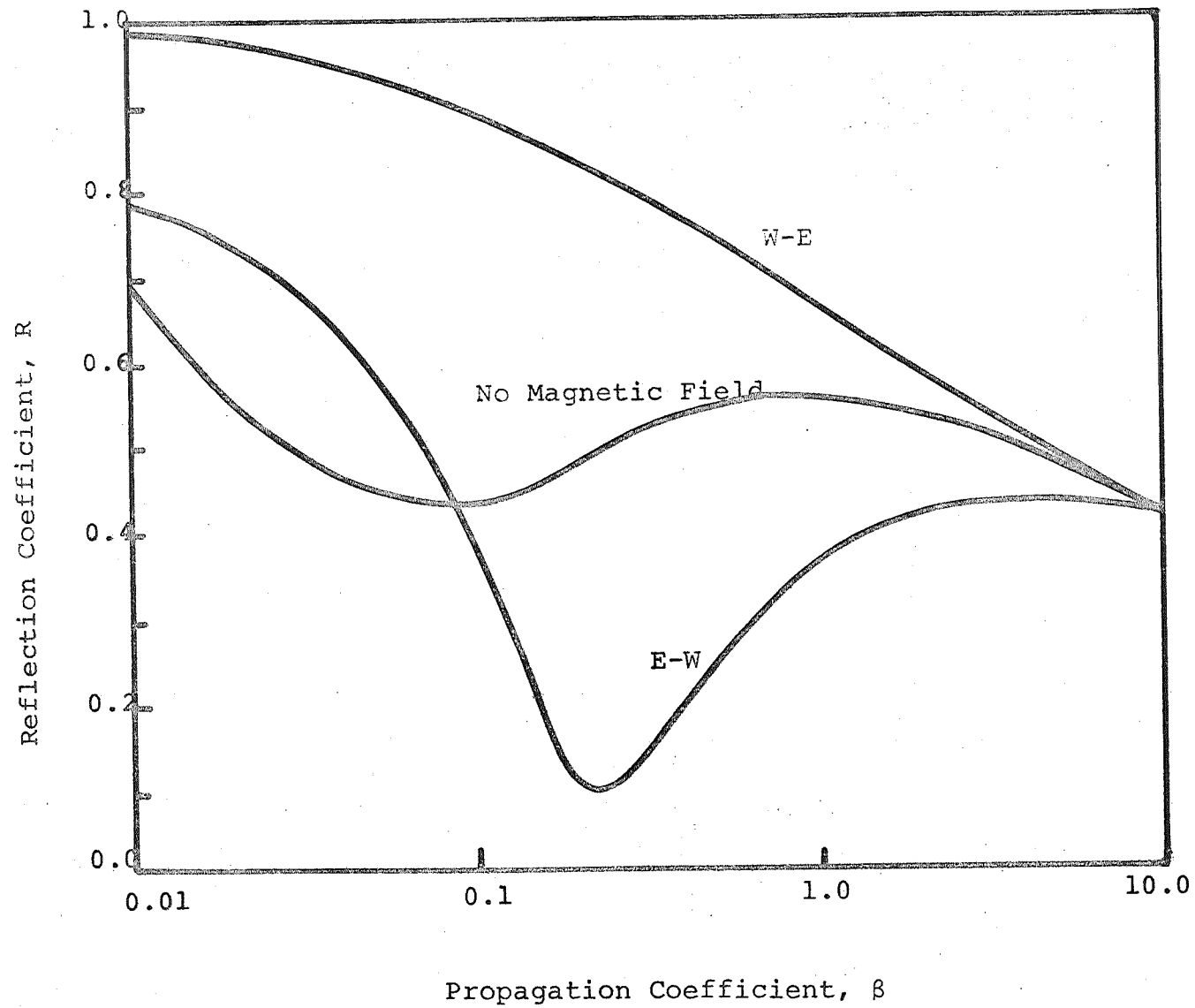


Figure 1 The Reflection Coefficient from the Ionosphere  
as a Function of Propagation Coefficient

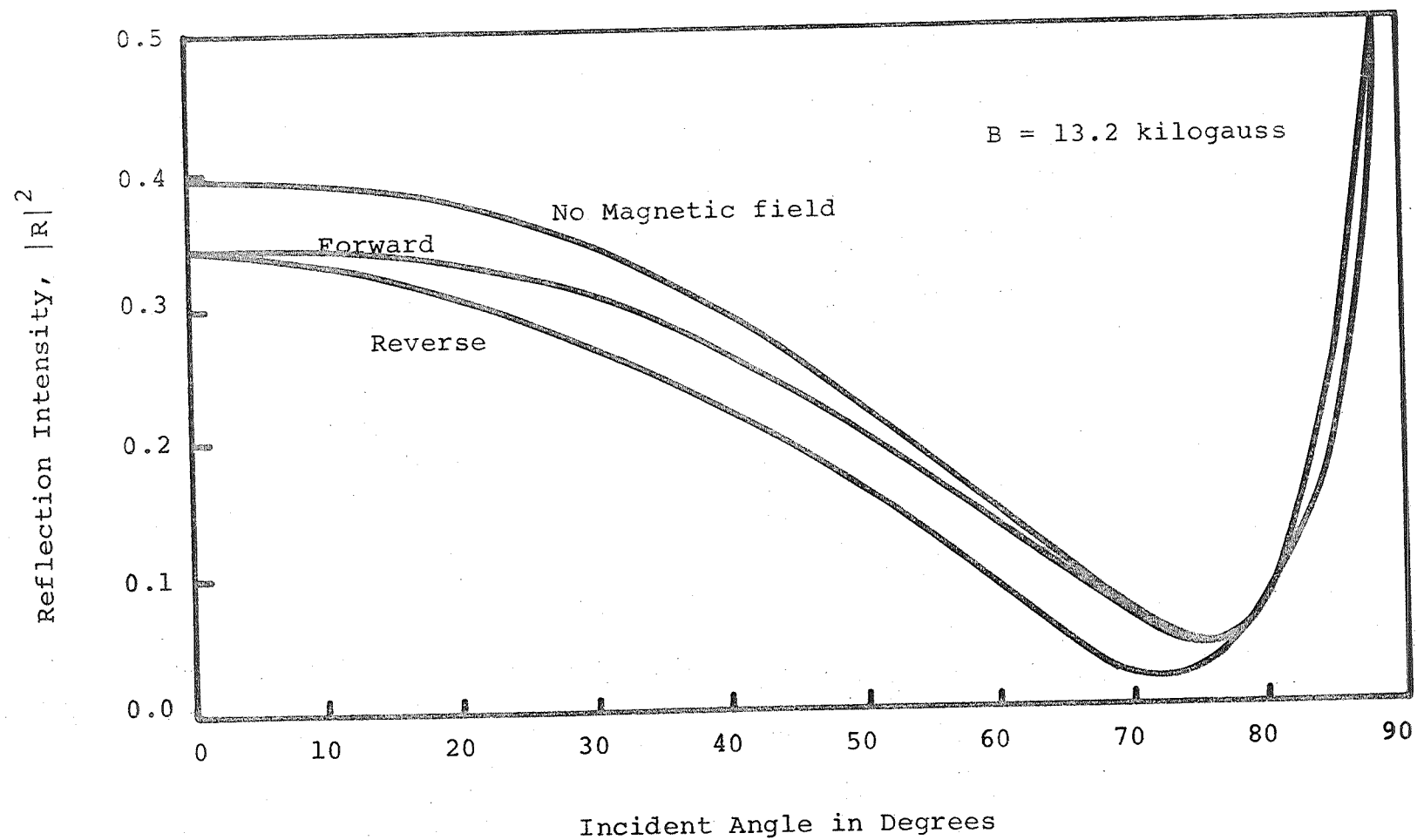


Figure 2 Theoretical Reflection Intensity from GaAs at 92GHz as a Function of Incident Angle



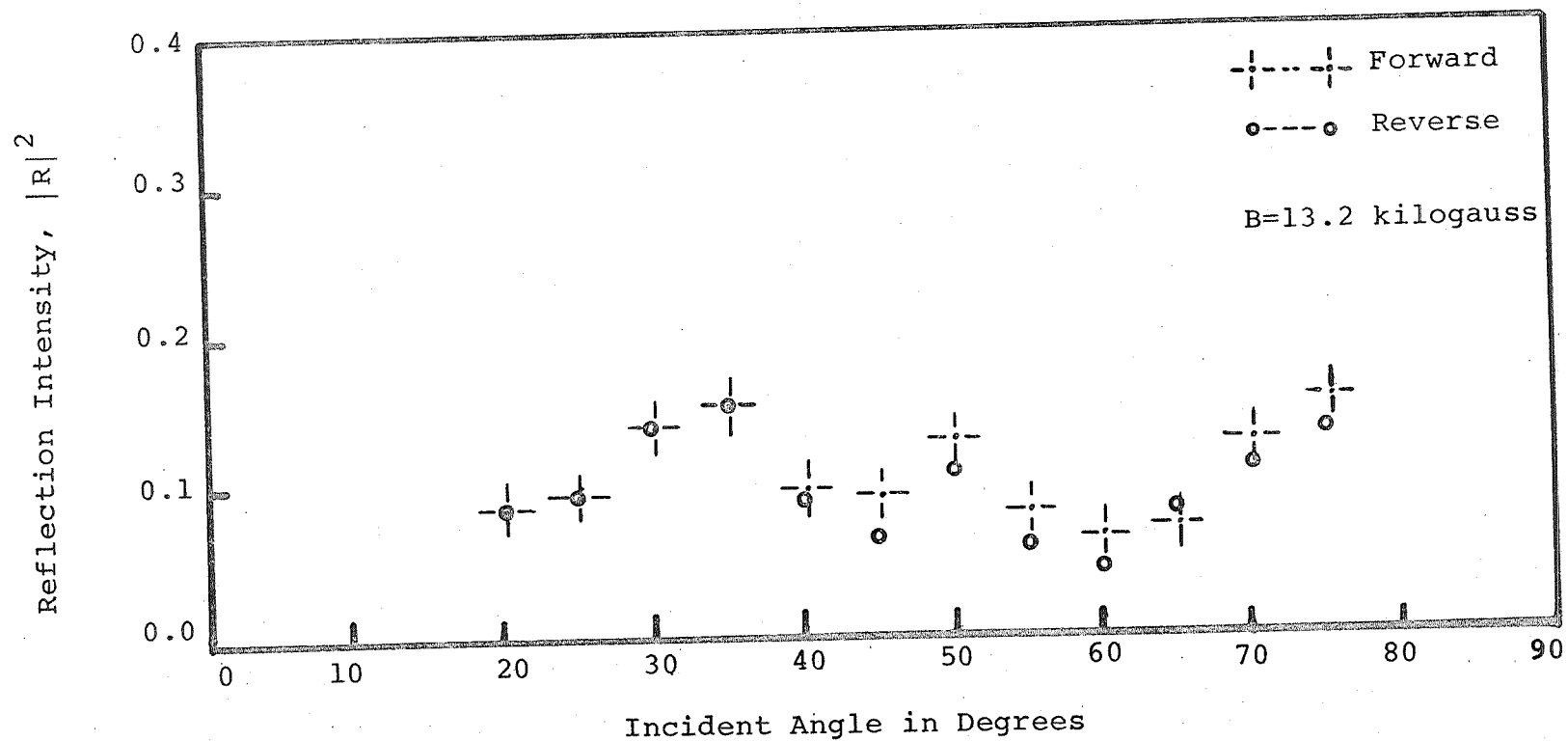


Figure 3 Experimental Reflection Intensity from GaAs at 92GHz as a Function of Incident Angle

whereas theory predicts 8.7db forward loss and 10.9db reverse loss, as shown in Fig. 2 and 3. Even for other choices of semiconductor parameters  $\theta$ ,  $n$ ,  $\mu$ ,  $B$  there is high forward loss and small reverse isolation, and this device does not look promising for device applications. However, N.F. Barber and D.D. Crombie [1] have calculated the reflection coefficient for W-E and E-W propagation when the angle of incident is  $78.5^\circ$  and obtained 1.6db forward loss and 21db reverse loss for the case  $\omega=10^5$ ,  $\omega_c=5 \times 10^6$ ,  $\omega_p=10^6/\text{sec}$  and  $v=5 \times 10^5 - 10^8/\text{sec}$  as shown in Fig. 1. We conclude that small nonreciprocal effect observed by J.M. Seaman is due to the large difference between the vacuum and lattice dielectric constants of GaAs. Thus we consider placing a slab of dielectric on top of the semiconductor.

Section 2-2 develops the theory of nonreciprocal reflection for a plane boundary between the solid state plasma and dielectric media when electric field is polarized in the plane of incidence, and the magnetic field perpendicular to the plane of incidence. The experimental apparatus and the procedure used to measure the nonreciprocal reflection for the surface of solid state plasma are given in section 2-3. In section 2-4 the correlation between experimental results and theory is discussed. Section 2-5 presents conclusions and future plans of our course of study.

## 2.2 Theoretical Derivation of Reflection Coefficient

We consider the reflection of a plane wave from a homogeneous solid state plasma bounded by a dielectric material. Defining

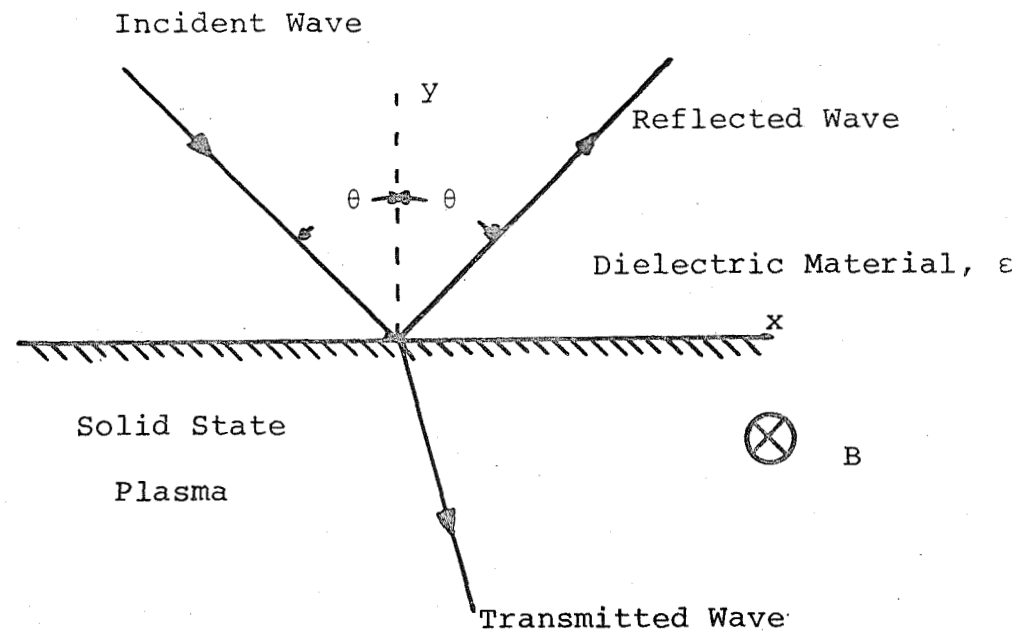


Figure 4 The Coordinate System for Reflection at the Plane Interface between a Solid State Plasma ( $y < 0$ ) and a Dielectric Material ( $y > 0$ )

Cartesian coordinates as shown in Fig. 4, a homogeneous solid state plasma occupies the space  $y > 0$  while dielectric material occupies the space  $y < 0$ . The case of an arbitrary orientation of the uniform dc magnetic field has first been considered by H. Bremmer [4], leading to very complicated results. However approximate and useful results for such cases have been obtained [5,6,7]. When the magnetic field is applied parallel to the  $z$  axis, it is possible to obtain the quasi static solutions of this boundary value problem. The calculation of the reflection coefficient for a plane wave between solid state plasma and a dielectric material, when the wave propagation is essentially transverse to the magnetic field, is shown in Appendix A.

When the electric field is in the plane of incidence, the reflection coefficient at the boundary of the solid state plasma is given by

$$R = \frac{\cos \theta - \frac{\epsilon}{\epsilon_0} \left[ A \left( \frac{\epsilon_0}{\epsilon} \frac{1}{A} - \sin^2 \theta \right)^{\frac{1}{2}} + D \sin \theta \right]}{\cos \theta + \frac{\epsilon}{\epsilon_0} \left[ A \left( \frac{\epsilon_0}{\epsilon} \frac{1}{A} - \sin^2 \theta \right)^{\frac{1}{2}} + D \sin \theta \right]} \quad (2-1)$$

and the transmission coefficient is given by

$$T = 1+R = \frac{2 \cos \theta}{\cos \theta + \frac{\epsilon}{\epsilon_0} \left[ A \left( \frac{\epsilon_0}{\epsilon} \frac{1}{A} - \sin^2 \theta \right)^{\frac{1}{2}} + D \sin \theta \right]} \quad (2-2)$$

where  $\theta$  is incident angle,  $\epsilon$  is dielectric constant of dielectric media and,  $A$  and  $D$  are components of the inverse relative

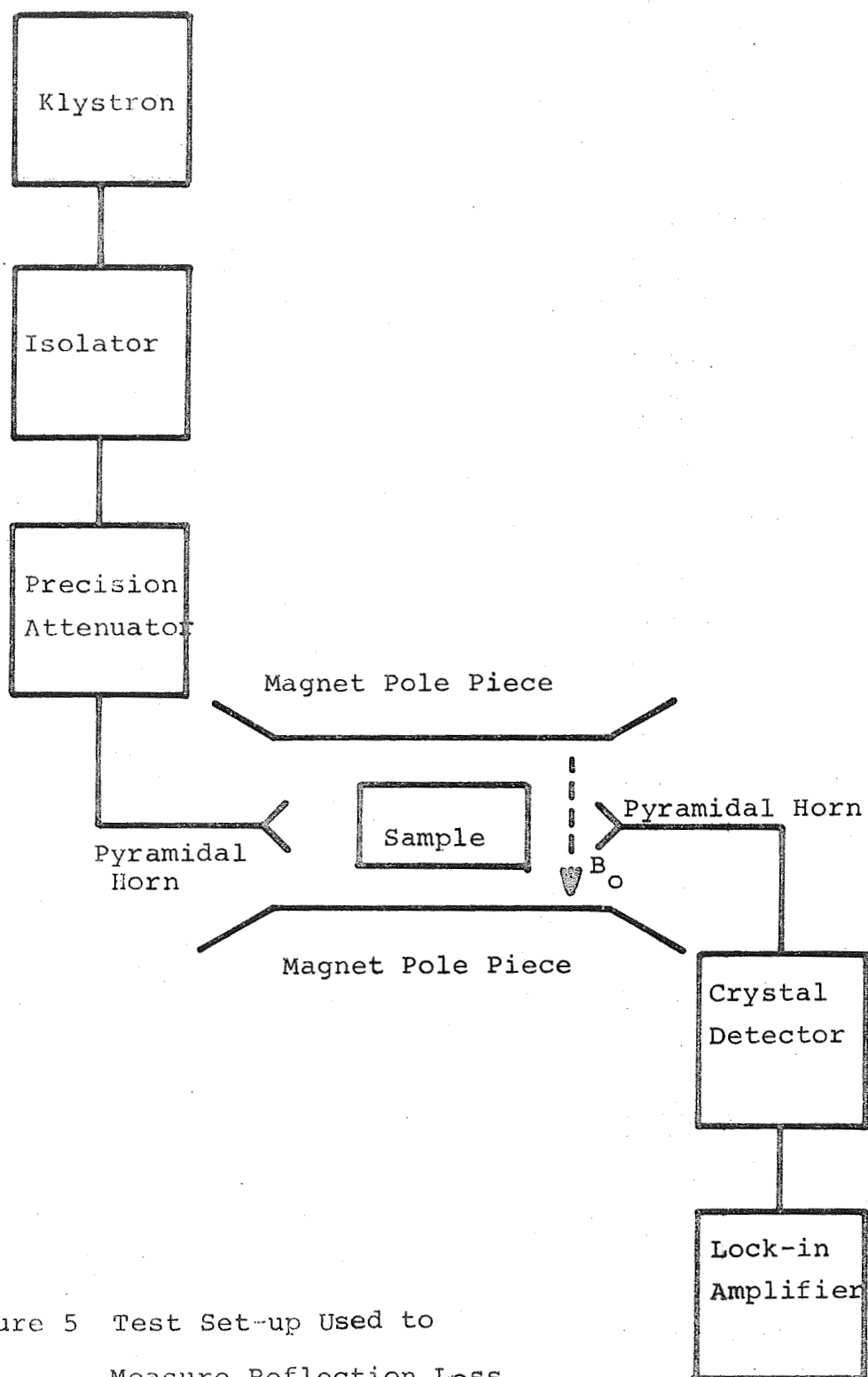


Figure 5 Test Set-up Used to Measure Reflection Loss from Solid State Plasma

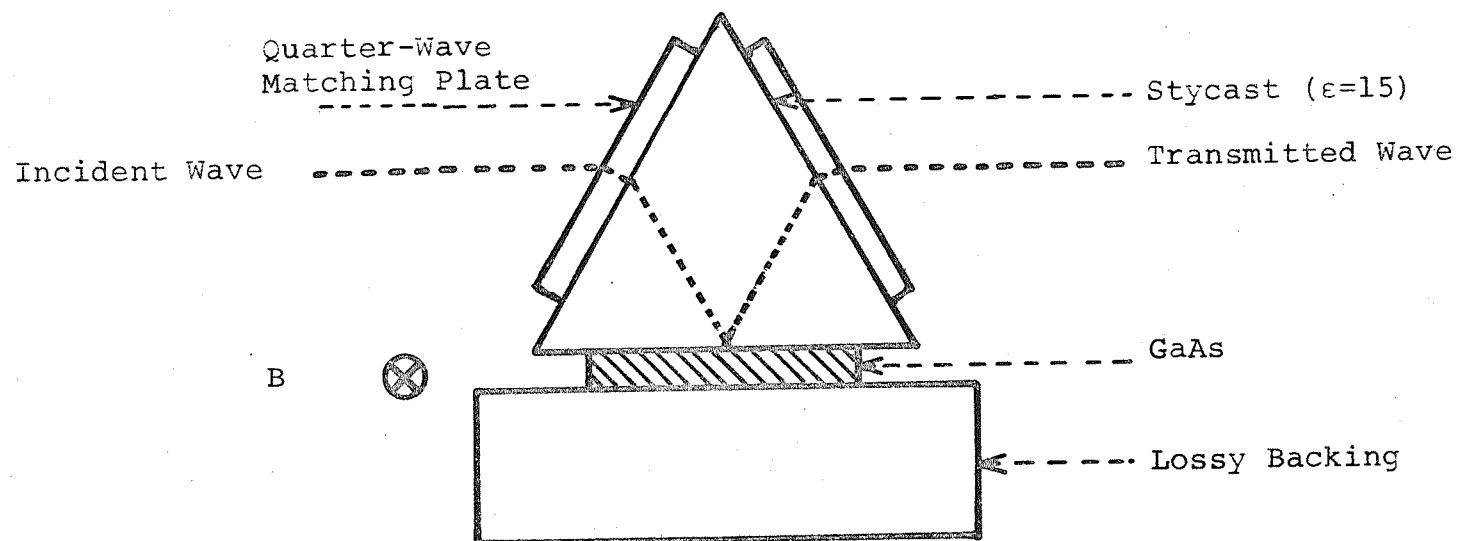


Figure 6 GaAs Reflection Isolator

dielectric tensor of the solid state plasma

$$K^{-1} = \begin{vmatrix} A & -D & 0 \\ D & A & 0 \\ 0 & 0 & B \end{vmatrix} \quad (2-3)$$

With the aid of a computer we calculated the reflection coefficients for a plane boundary between solid state plasmas and a dielectric material as a function of incident angle  $\theta$  and as a function of the magnetic field B.

### 2.3 Experiment Procedure

The experimental apparatus shown in Fig. 5 is designed to measure the reflection from the surface of n-type GaAs covered by a dielectric medium. Since theory predicts optimum isolation for the incident electric field at an angle  $\theta = 60^\circ$  as shown in Fig. 10 and 11, a  $60^\circ$  pyramidally-cut dielectric (Stycast  $\epsilon = 15\epsilon_0$ , Emerson and Cuming) was used as a "lossless" dielectric medium. The semiconductor used for the experiment is n-type GaAs which was mechanically and chemically ( $H_2SO_4(4) - H_2O_2(1) - H_2O(1)$ ) polished and was mounted on the bottom of pyramidally-cut Stycast as shown in Fig. 6. Quarter-wave matching plates were placed on the incident and transmitted sides.

The skin depth  $\delta$  inside GaAs was calculated theoretically using Eq. (A-16) given in Appendix A

$$\delta = -\text{Imag} \left[ \frac{k_o^2}{A} - k^2 \sin^2 \theta \right]^{-\frac{1}{2}} \quad (2-4)$$



where  $k_o = \omega \sqrt{\mu_o \epsilon_o}$  ,  $k = \omega \sqrt{\mu_o \epsilon}$  ,

$\epsilon$  is the dielectric constant of a dielectric medium and  $A$  is one of the diagonal components of the inverse relative dielectric tensor of the solid state plasma given in Eq. (2-3). The theoretical skin depths inside GaAs as a function of magnetic field and as a function of incident angle are shown in Fig. 7 and 8. Since the GaAs wafer was only one skin depth thick (0.5mm thick, 2cm in diameter), Eccosorb AN-72 was used as a low reflective backing. This device was placed at 300°K in the air gap of an electromagnet providing up to 16 kilogauss. Horns were used to provide 94 GHz incident "plane" wave whose electric field is polarized in the plane of incidence, and as a detector pickup. A lock-in amplifier was used to amplify and read the signal from the crystal detector. In order to reduce the effects of stray signals, a window made out of Al foil was placed on the pyramid at the side of incidence. Total insertion loss is somewhat difficult to measure because of use of pyramidal horns. The net insertion loss from absorption due to GaAs was, however, estimated by measuring the difference of reflected power using GaAs, and using a metallic inductor.

Another isolator operated at 94 GHz and at 300°K using InSb was considered and is shown in Fig. 9. From the theoretical calculation shown in Fig. 13, the angle of incidence at which optimum performance could be obtained turns out to be about

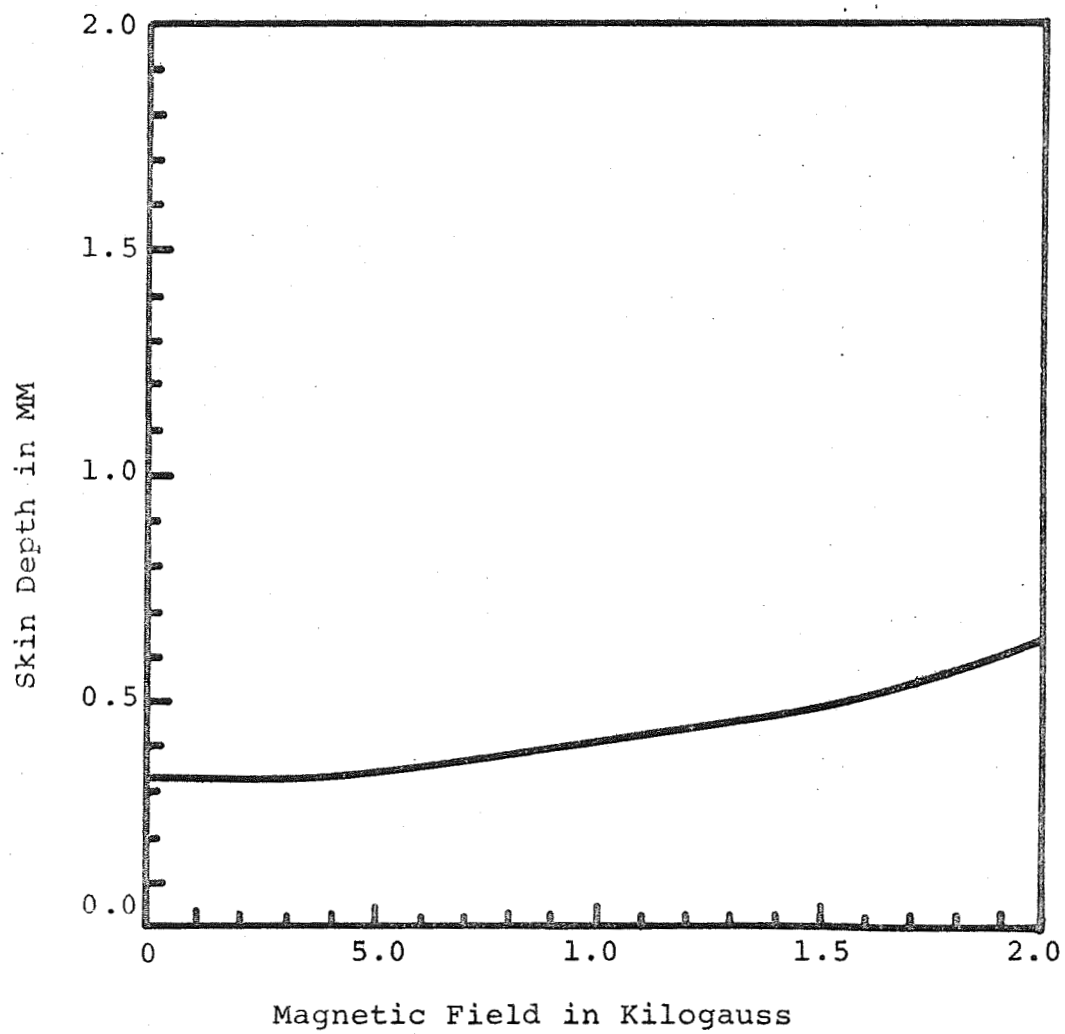


Figure 7 Theoretical Skin Depth Inside GaAs as a Function of Magnetic Fields

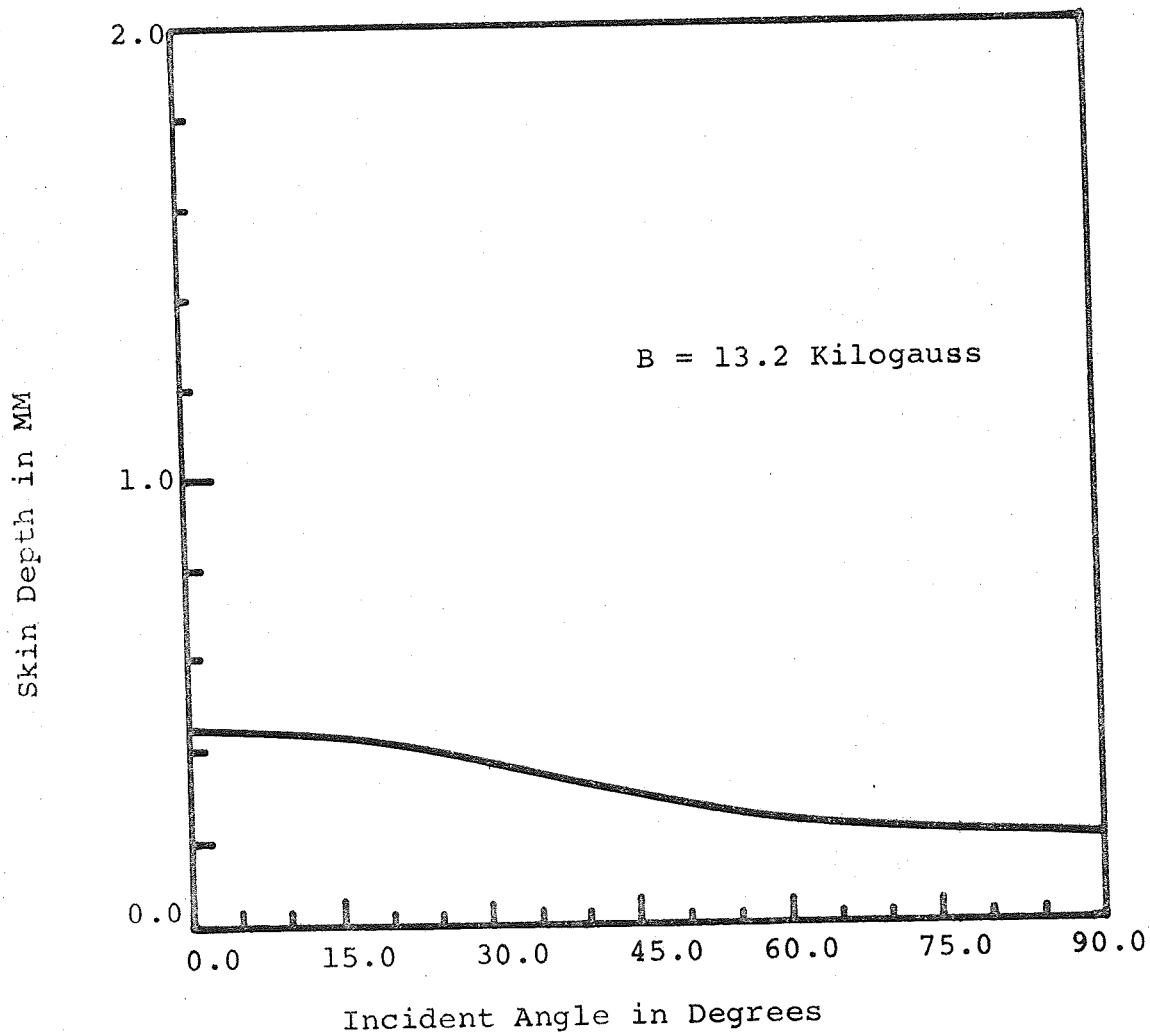


Figure 8 Theoretical Skin Depth Inside GaAs as a  
Function of Incident Angle

15

Rutile  
( $\text{TiO}_2$ )

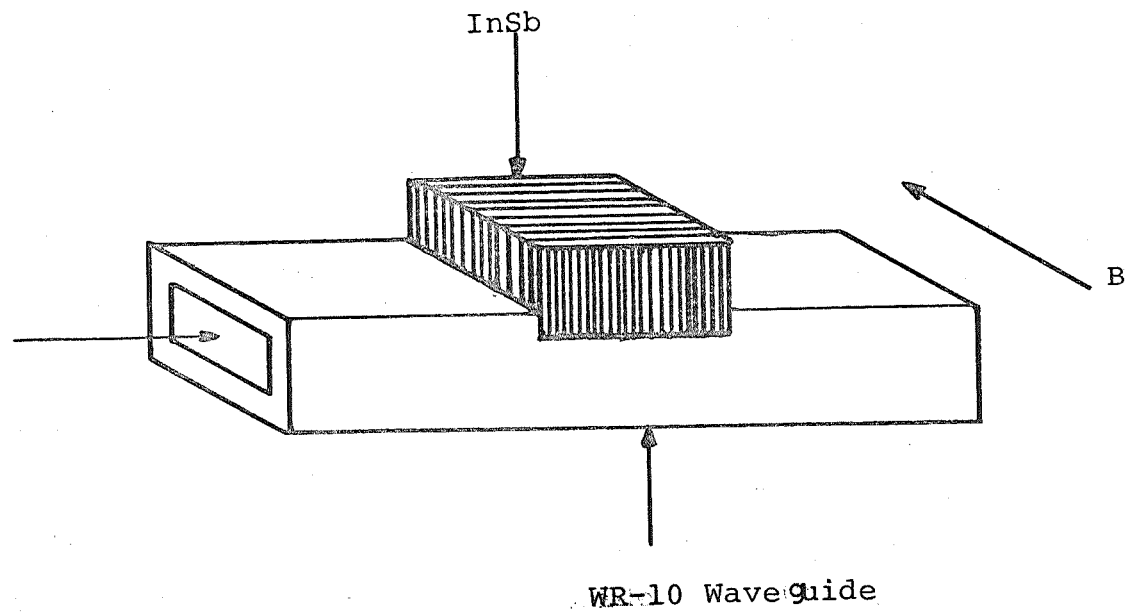


Figure 9 InSb Waveguide Isolator

80°. By using InSb as the top wall of the wave guide filled with high dielectric material (rutile,  $\epsilon \approx 40\epsilon_0$ ), the bending of the wave front may give the same configuration as the case when incident angle of electric field is around 80°.

## 2.4 Experimental Results

### 2.4.1 Measurement of GaAs and InSb parameters

Detailed experiments have been performed in GaAs which indicate that the effective mass is taken to be  $0.07 m_0$  [8] and the relative dielectric constant is assumed to be 12.5 [9]. The mobility and free carrier concentration were measured at 300°K by the Van der Pauw method, [10] which does not depend on sample geometry. The parameters of GaAs used in the experiments is shown below.

$$\begin{aligned} m^* &= 0.07 m_0 \\ \epsilon_r &= 12.5 \epsilon_0 \\ \mu_e &= 6100 \text{ cm}^2/\text{volt-sec} \\ n &= 7.1 \times 10^{14} / \text{cm}^3 \end{aligned}$$

C.A. Hogarth [11] quotes experimental results for the effective mass of InSb as  $0.0155 m_0$  or  $0.0145 m_0$  and the relative dielectric constant 17.5. From Faraday rotation experiments performed in this laboratory [12], the relative dielectric constant was found to be 16.0. By performing the Van der Pauw measurement [10] at 300°K, the parameters of InSb used in this experiment are shown below.

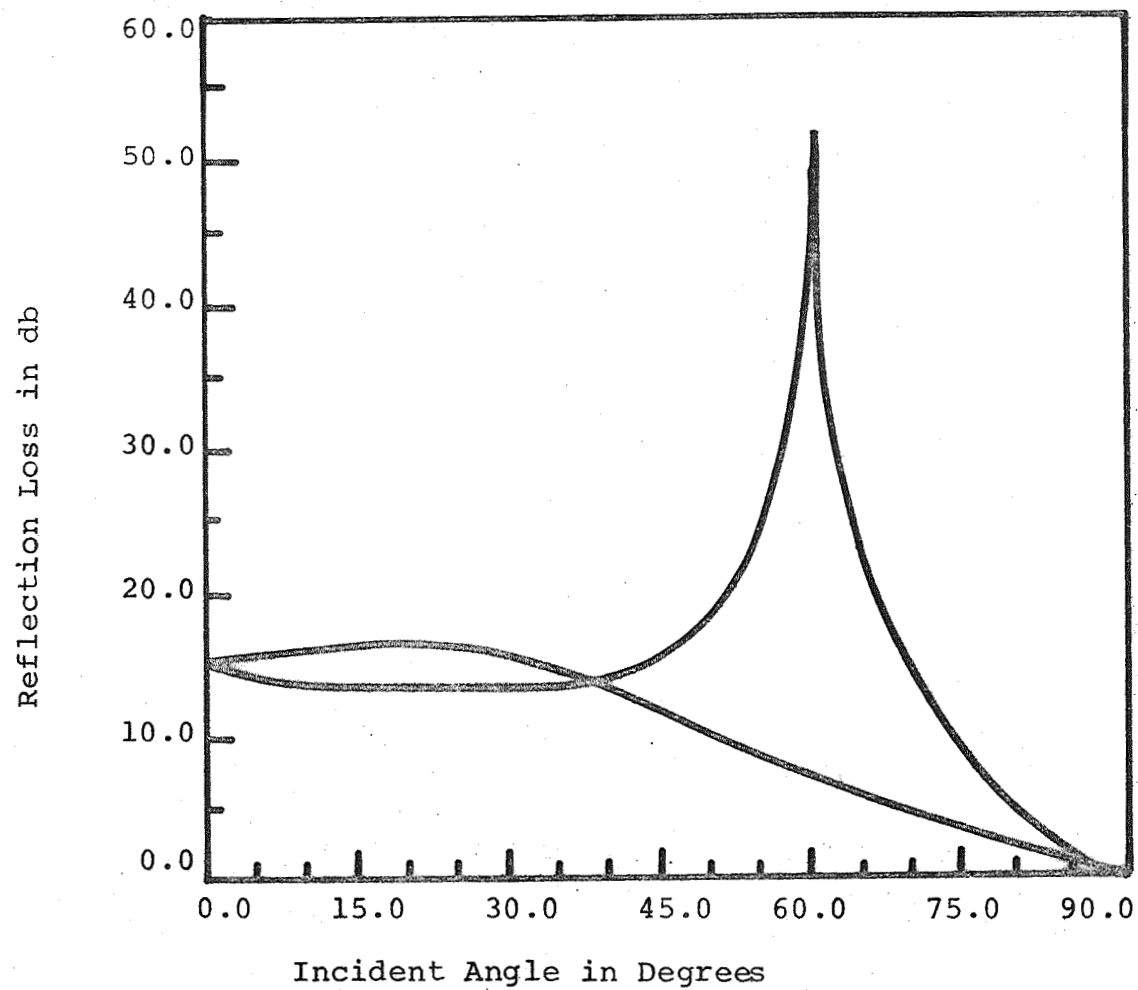


Figure 10 Theoretical Reflection Loss for GaAs Reflection  
Isolation at 94GHz as a Function of Incident Angle

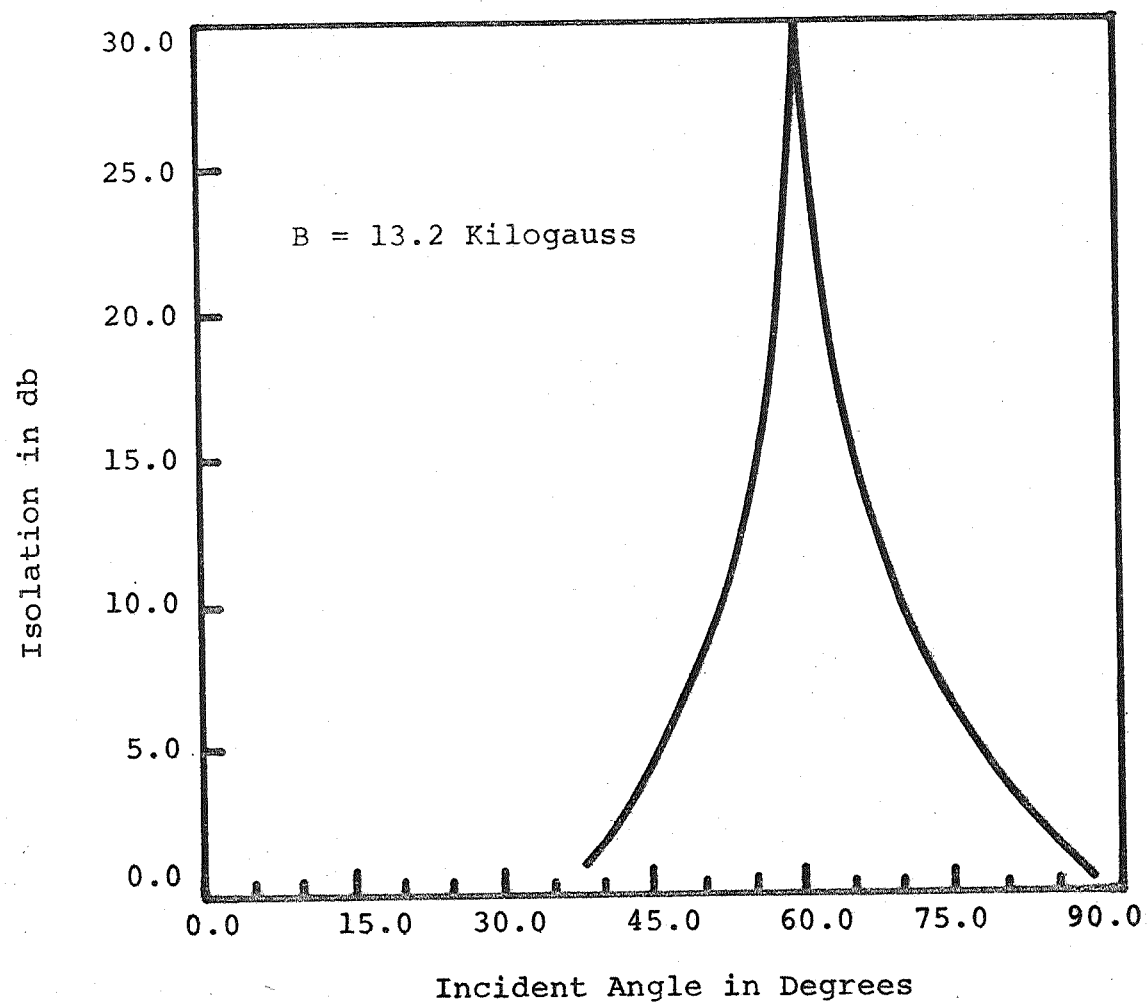


Figure 11 Theoretical Isolation of GaAs Reflection Isolator at 94GHz as a Function of Incident Angle



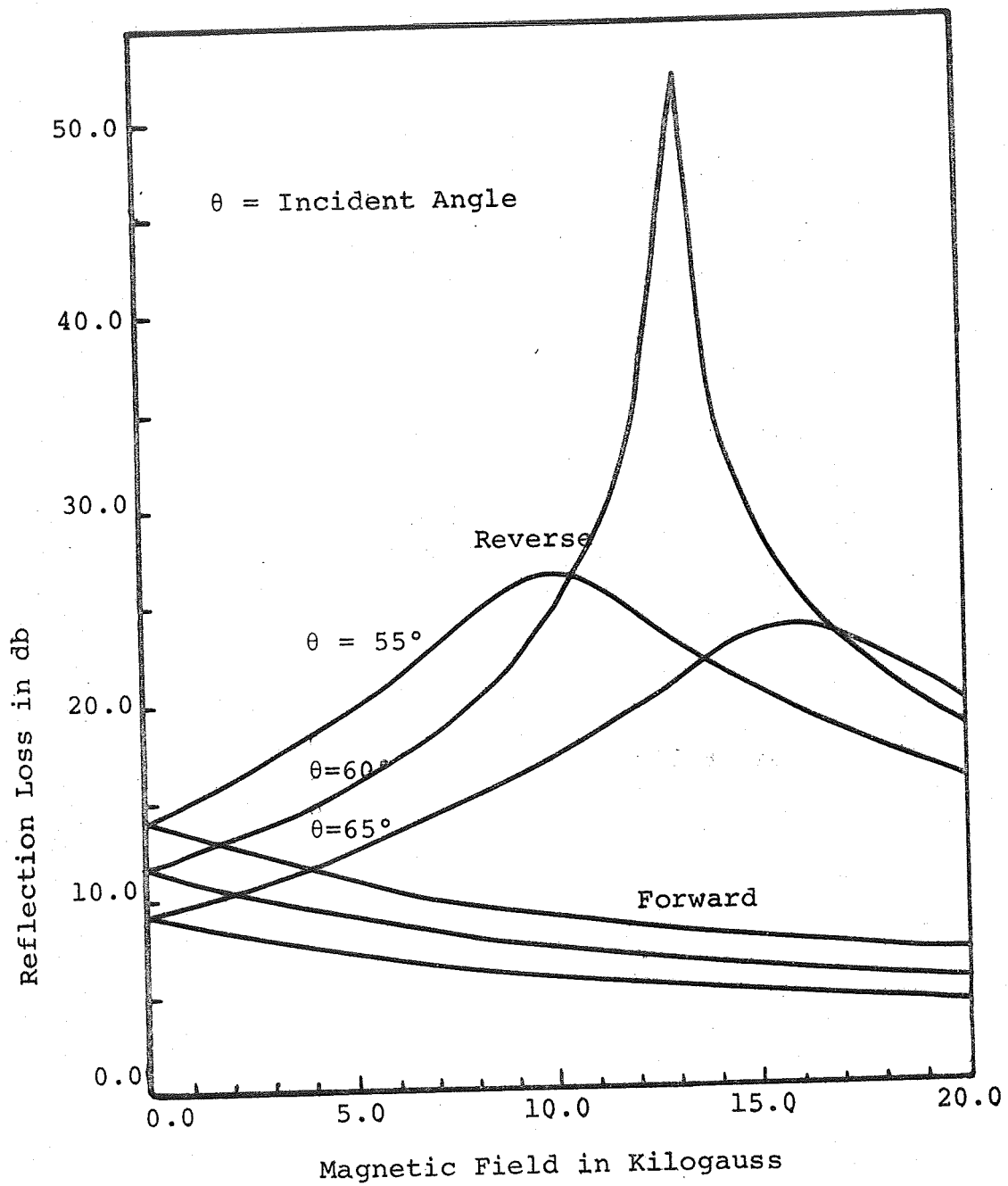


Figure 12 Theoretical Reflection Loss of GaAs  
Reflection Isolator at 94GHz as a  
Function of Magnetic Field

$$\begin{aligned}
m^* &= 0.015 m_0 \\
\epsilon_l &= 16.0 \epsilon_0 \\
\mu_e &= 7 \times 10^4 \text{ cm}^2/\text{volt-sec} \\
n &= 1.35 \times 10^{16} / \text{cm}^3
\end{aligned}$$

#### 2.4.2 Comparison of Experimental Results with Theory

Fig. 10 shows theoretical reflection loss from GaAs with a dielectric layer ( $\epsilon=16\epsilon_0$ ) for electric fields polarized in the plane of incidence at 94 GHz and at 300°K with a uniform magnetic field of 13.2 kilogauss as a function of incident angle  $\theta$ . The theoretical results of isolation from the GaAs surface covered by a dielectric material ( $\epsilon = 16\epsilon_0$ ) as a function of incident angle  $\theta$  is shown in Fig. 11. Fig. 12 shows the theoretical variation of the reflection loss as a function of the uniform magnetic field B with fixed incident angles ( $\theta = 55.0^\circ$ ,  $60.0^\circ$  and  $65.0^\circ$ ). Also InSb with a dielectric layer ( $\epsilon=40\epsilon_0$ ) was used for the calculation of reflection coefficient at 94 GHz and at 300°K with uniform magnetic field of 13.2 kilogauss, and its theoretical reflection loss as a function of incident angle  $\theta$  is shown in Fig. 13. The theoretical calculations of reflection coefficient are also performed for infrared wavelengths,  $337\mu$  and  $118\mu$  from HCN and  $H_2O$  laser, respectively. The theoretical reflection loss for a plane boundary between InSb and a dielectric layer ( $\epsilon=30\epsilon_0$ ) at  $\lambda=337\mu$  and at 300°K with uniform magnetic field of 13.2 kilogauss as a function of incident angle is shown in

Fig. 14. Similarly Fig. 15 and 16 show the theoretical reflection loss for a plane boundary between InSb and a dielectric layer ( $\epsilon=50\epsilon_0$ ) at  $\lambda=118\mu$  and at  $300^\circ\text{K}$  as a function of incident angle with uniform magnetic field of 13.2 and 16.0 kilogauss, respectively.

Experimental results of the isolation from a GaAs surface covered by a dielectric-material ( $\epsilon=15\epsilon_0$ ) as a function of incident angle  $\theta$  is shown in Fig. 17. This experiment was conducted at 94GHz are at  $300^\circ\text{K}$  with the constant uniform magnetic field of 13.2 kilogauss as was theoretical calculation. Fig. 18 shows the experimental variation of reflection loss as a function of the uniform magnetic field with the fixed incident angles ( $\theta=56.2^\circ$  and  $57.5^\circ$ ).

Isolation of 11.0db with 11.0db insertion loss was observed for the signal at an incident angle of  $57.5^\circ$  whereas theory predicts 54db isolation with 9db insertion loss at an incident angle of  $60^\circ$  as shown in Fig. 10 and 11. The considerable deviation between these is probably due to non-plane wave behavior of the incident wave and non-uniform material parameters. The window used to reduce stray reflection and transmission is only about  $5 \times 7$  wavelengths. This non-plane wave behavior caused by the small window might have smeared out the sharpness of the isolation curve shown in Fig. 10 and 11. This was also confirmed from the fact that a much smaller window, 3 wavelengths square, completely destroyed the nonreciprocal phenomena. Also a substantial beam angle of  $4^\circ$  to  $6^\circ$  of the transmitting

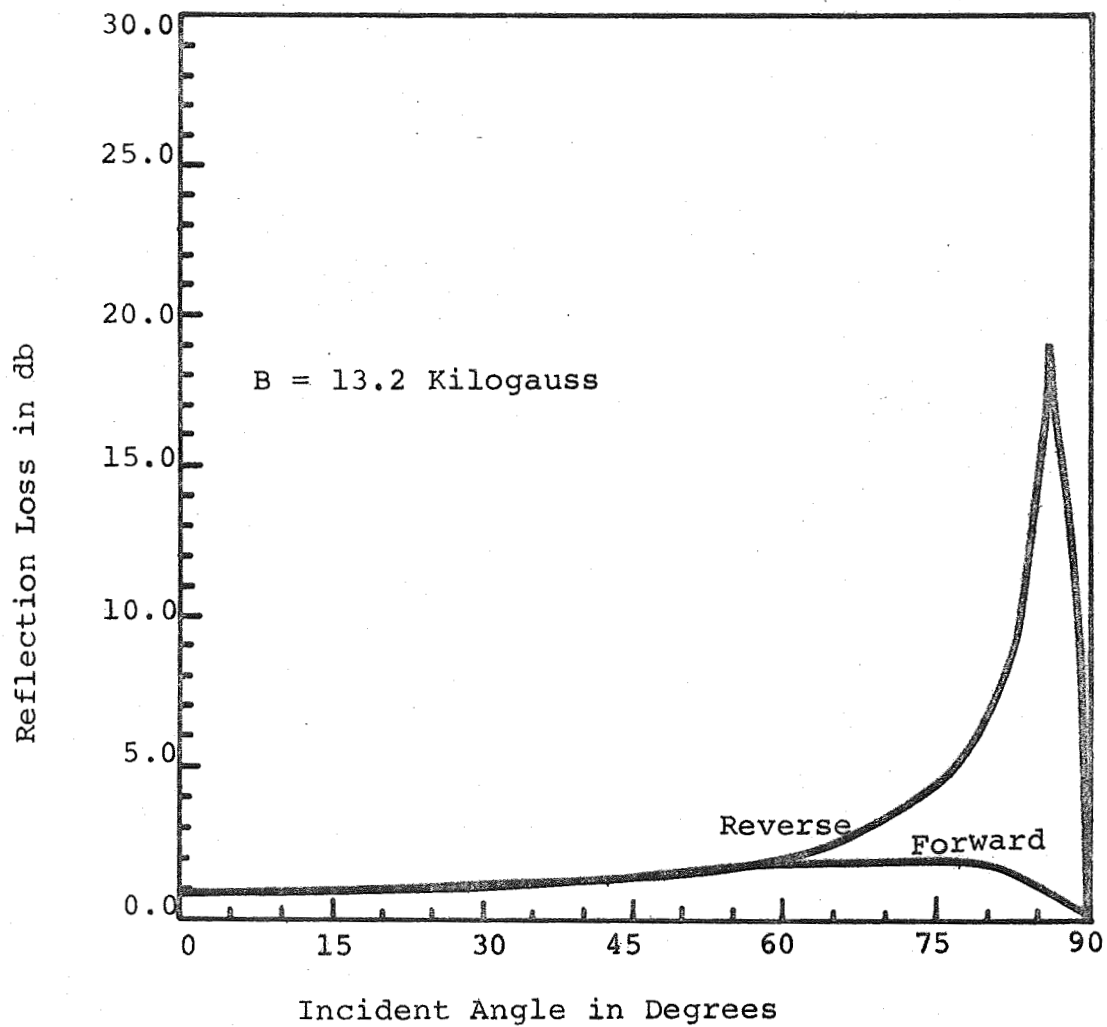


Figure 13 Theoretical Reflection Loss for InSb  
Reflection Isolator at 94GHz as a  
Function of Incident Angle

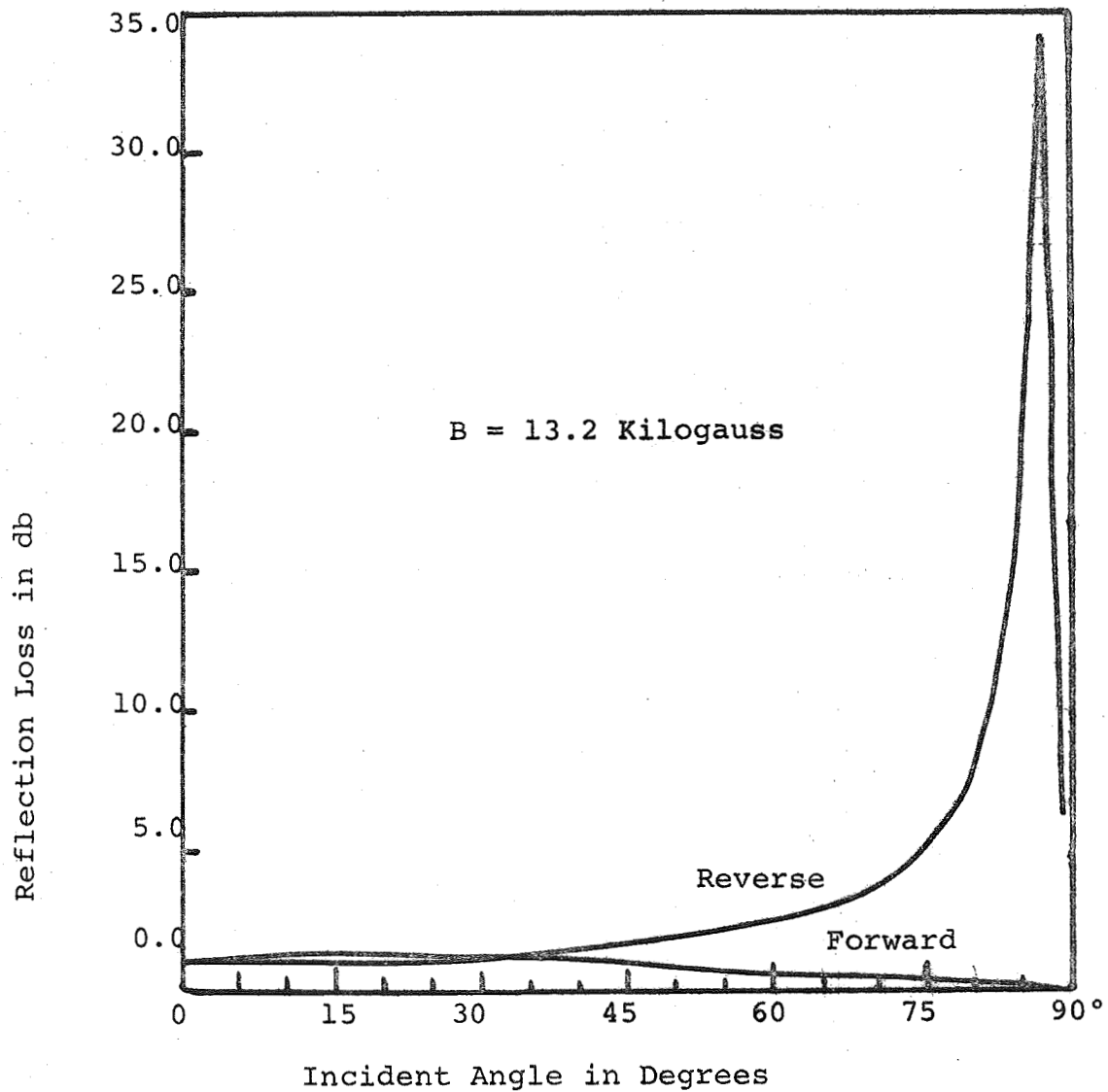


Figure 14 Theoretical Reflection Loss of InSb  
Reflection Isolator at  $\lambda=337\mu$  as a  
Function of Incident Angle

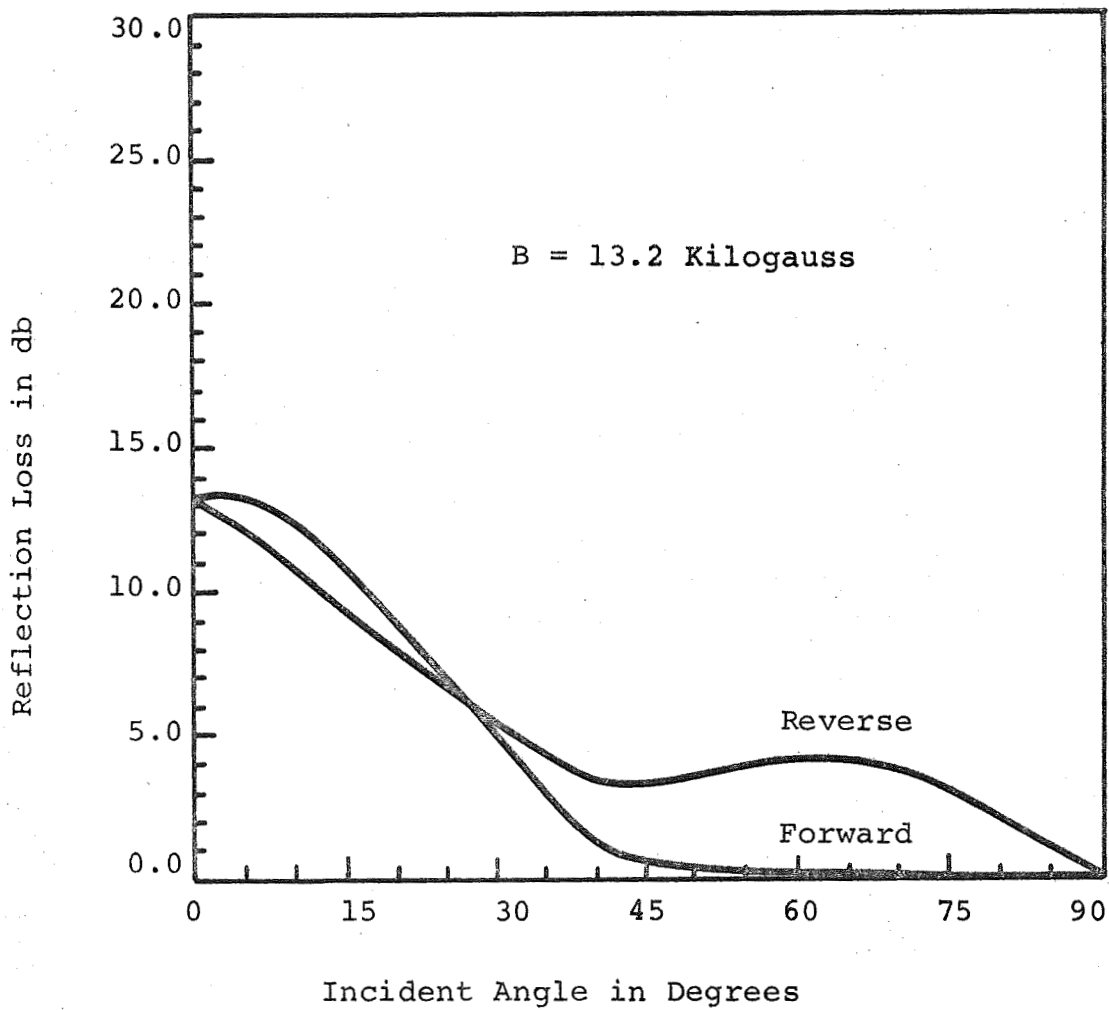


Figure 15 Theoretical Reflection Loss of InSb  
Reflection Isolator at  $\lambda=118\mu$  as a  
Function of Incident Angle

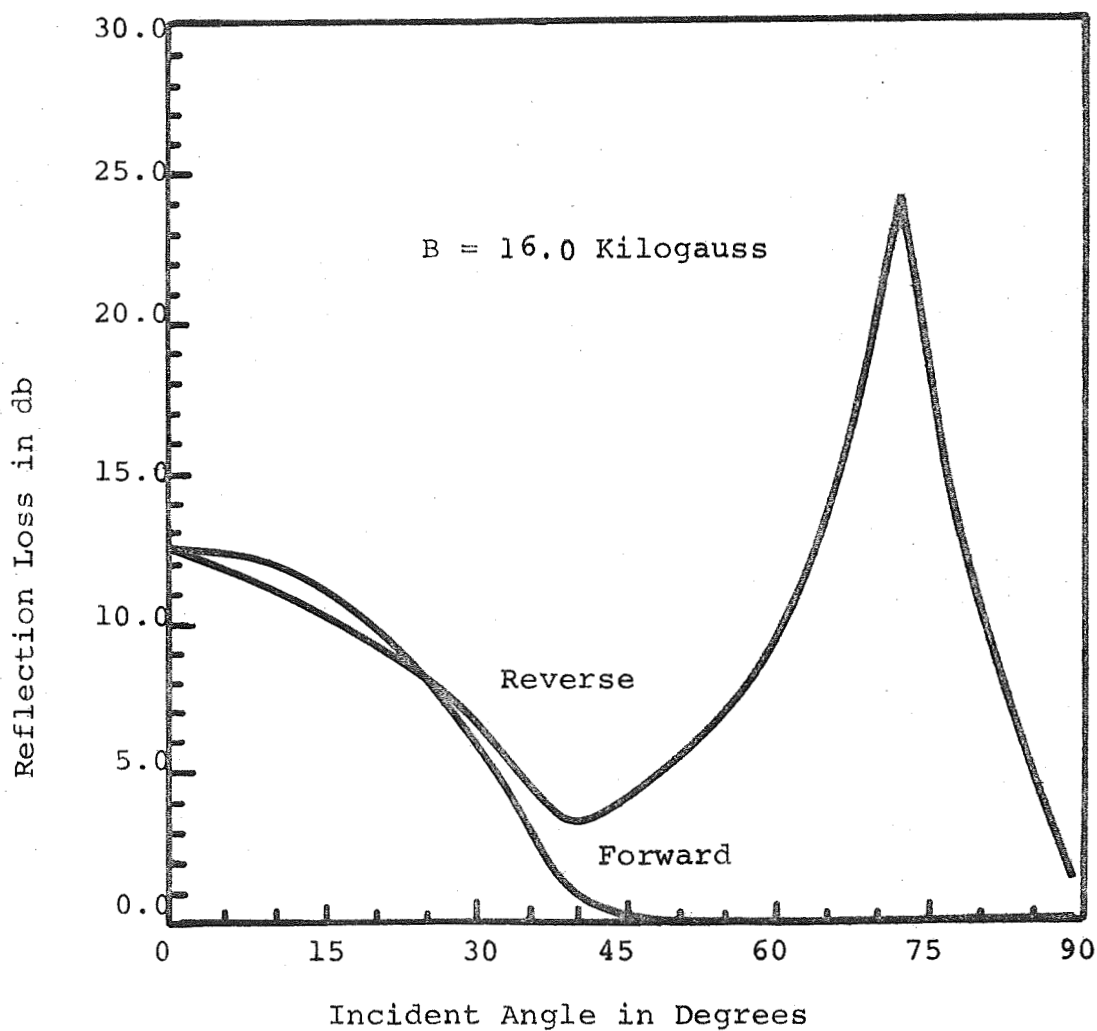


Figure 16 Theoretical Reflection Loss of InSb Reflection Isolator at  $\lambda=118\mu$  as a Function of Incident Angle



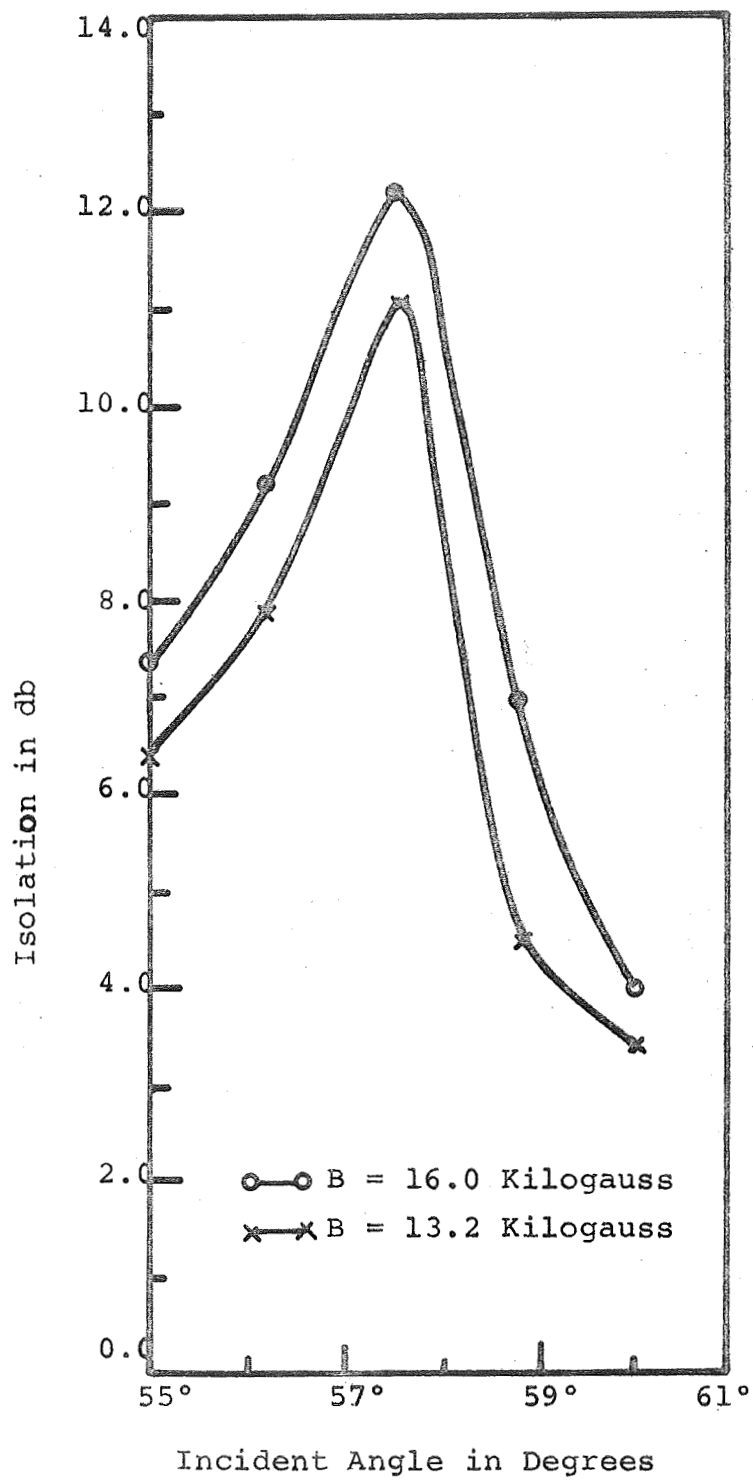


Figure 17 Experimental Isolation of GaAs Reflection Isolator at 94GHz as a Function of Incident Angle

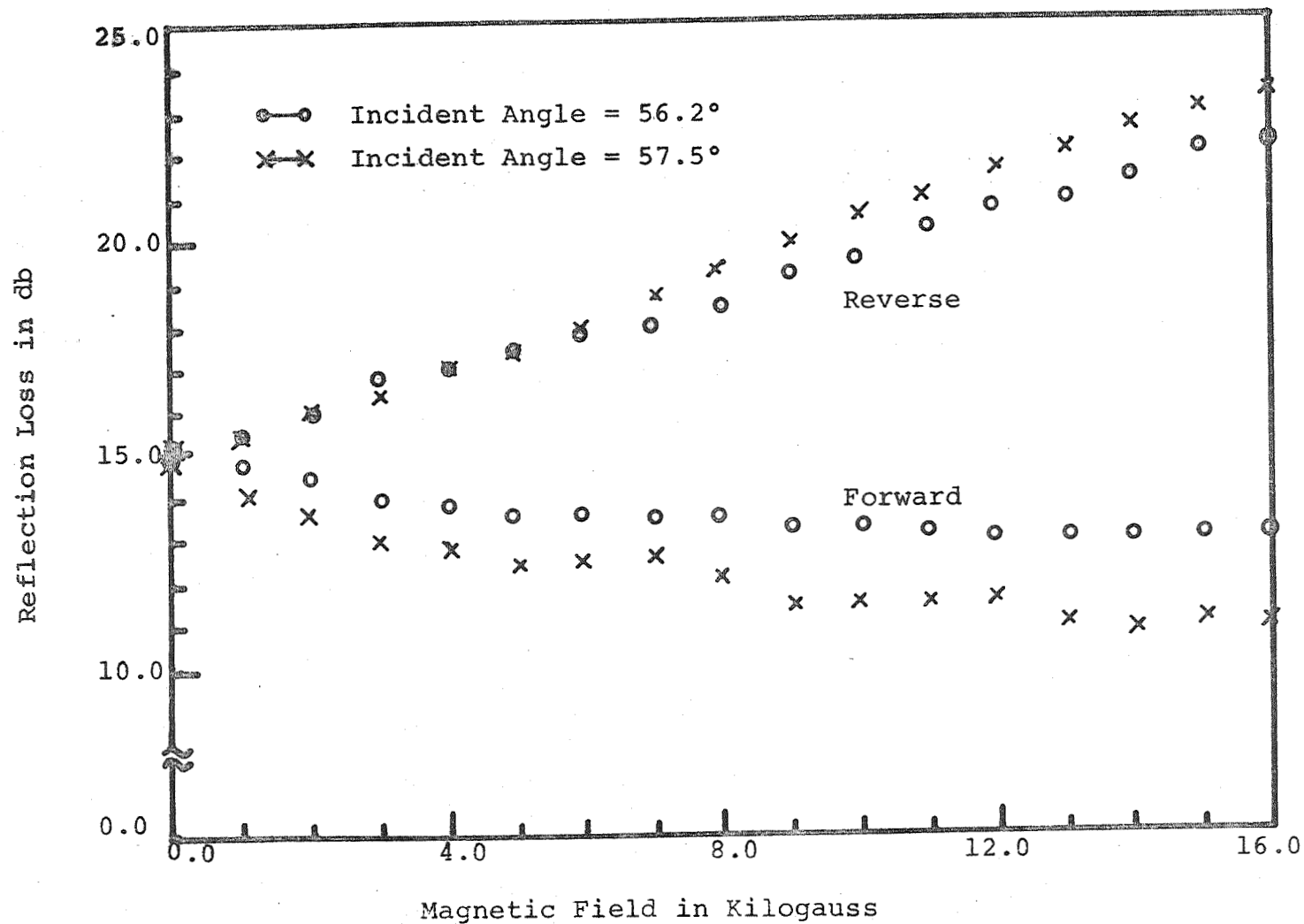


Figure 18 Experimental Reflection Loss of GaAs Reflection Isolator at 94GHz as a Function of Magnetic Field

and receiving pyramidal horns causes significant error, since the reflection coefficient changes rapidly with incident angle. The reflection from the back side of the GaAs (0.5mm thick) might have washed out some nonreciprocal nature, although the Eccosorb backing was used to reduce this reflection.

The isolator using the InSb as the top wall of a wave guide shown in Fig. 9 was also tried without success. The wave guide was filled by the rutile ( $TiO_2$ ) which has relative dielectric constant of around 50 and operated at 94GHz and at 300°K with uniform transverse magnetic field up to 16 kilogauss. Using this device, we could not observe any nonreciprocal phenomena. This might be due to a number of factors. First, the bending of wave front might have not been a desired angle, although incident angle 80° is required from the theory as shown in Fig. 11. Second, the excitation of higher modes inside the rutile might have cancelled the nonreciprocal phenomena. Internal reflections in the rutile also might have caused problems. Exact theoretical investigation for the configuration is now being considered.

## 2.5 Conclusions and Future Plans

The reflection coefficient for a plane boundary between a solid state plasma and a dielectric material has been studied for the incident signal polarized in the plane of incidence and traveling perpendicular to the magnetic field. Theoretical and experimental results indicate promising device applications

for isolators operated at quasi-optical to optical frequencies and at room temperature.

We are preparing to do further experiments at 337, 118, and 27 microns using HCN and  $H_2O$  lasers. Careful selection of the solid state plasma (InSb, GaAs, and InAs) and a high dielectric material (rutile and etc.) will promise good performance as an isolator in optical systems.

### 3. Far Infrared Isolators Using Faraday Rotation

#### 3.1 Introduction

This research work is an extension of the project undertaken last year (14) in which we investigated the possible millimeter wave device applications of an electromagnetic plane wave propagating in a solid state plasma in a magnetic field. The magneto-optical effect encountered is the so called Faraday effect characterized by the rotation of the plane of polarization of an electromagnetic wave in the presence of a static longitudinal magnetic field.

The prior experiments were performed at a wavelength of 3.2mm and were found to be in good agreement with the theoretical calculations. The proposed experiments will be conducted at respectively 28 microns, 118 microns and 337 microns. The two first wavelengths correspond to cw laser lines of water vapor while the last one is the strongest emission line wavelength of the CN radical.

In the infrared region of the spectrum the optical properties of semiconductors are determined by the free carriers and by lattice vibrations.

#### 3.2 Theory

We consider first the simplified free carrier Faraday rotation theory (Appendix B, 12, 13, 14) treated in classical terms. The electron plasma simulating the semiconductor through which

the electromagnetic wave propagates is infinite in length and is immersed in a static magnetic field. Further assumptions can be derived from the two following conditions:

1. A sufficiently high magnetic field is applied to the semiconductor
2. The high frequency of the infrared radiation

namely,

$$\begin{aligned} \omega &> \omega_c & \omega_c &= \frac{eB_0}{m^*} \\ \omega^2 \tau^2 &\gg 1 & & \\ \omega_p^2 / \omega^2 &< 1 & \omega_p^2 &= \frac{ne^2}{\epsilon_l m^*} \end{aligned} \quad (B.17)$$

It is interesting to note that these are quite different from the microwave case where we had:

$$\begin{aligned} \omega &< \omega_c \\ \omega_c \tau &= \mu B_0 \gg 1 \\ \omega \omega_c &\gg \omega_p^2 \end{aligned}$$

Using the assumptions for the infrared case into the complete expression giving the propagation constant, one obtains after simplification the Faraday Rotation angle per unit length as

$$\theta = \frac{\omega_p^2 \omega_c}{2\omega^2} \sqrt{\epsilon_l \mu_0} \quad (B.21)$$

where

$\omega_p$  = plasma frequency

$\omega_c$  = cyclotron resonance frequency

$\omega$  = operating frequency

$\epsilon_l$  = dielectric constant of semiconductor sample

$\mu_0$  = permittivity of vacuum

The results of the computation are shown in Figure 19 for samples of InSb of concentration and of mobility that could be expected for room temperature operation. Rotation is seen, for low magnetic fields to have a linear dependence and to increase with higher carrier concentration for a constant magnetic field.

The model used in this computation can be seen to describe the case where no reflections are occurring at the boundaries of the semiconductor plasma. Such a scheme can be achieved by using impedance matching plates or coatings on the semiconductor slab. Then a Faraday rotator giving a  $45^\circ$  rotation for a field of 10 kG would show a loss L expressed by:

$$L = \frac{6.8}{\mu B} \left( \frac{\theta}{\pi/4} \right) \text{ db}$$

or with the above numbers for InSb at room temperature

$$L = 0.85 \text{ db.}$$

The low loss found with this scheme makes it attractive for device applications.



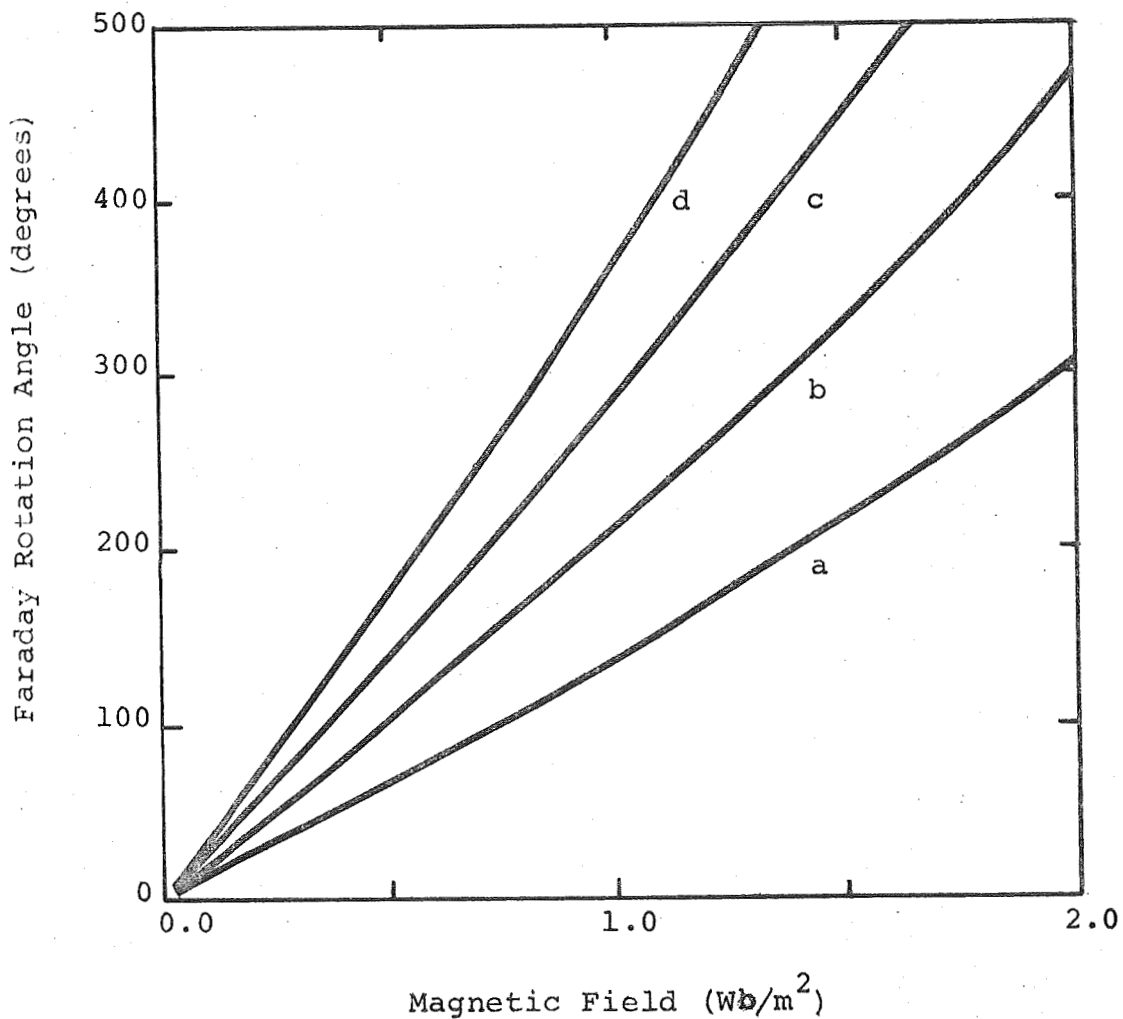


Fig. 19. Theoretical Faraday Rotation Angle

versus Magnetic Field

Computation Simulated for a sample of Indium Antimonide of various carrier concentrations at room temperature

- |                                        |                                        |
|----------------------------------------|----------------------------------------|
| a. $2.0 \cdot 10^{16} \text{ cm}^{-3}$ | c. $4.0 \cdot 10^{16} \text{ cm}^{-3}$ |
| b. $3.0 \cdot 10^{16} \text{ cm}^{-3}$ | d. $5.0 \cdot 10^{16} \text{ cm}^{-3}$ |

In the above analysis we have not taken into account the influence of multiple reflections at the boundaries of the solid state plasma. The effects of multiple reflections on the transmission properties of an infinite semiconductor sheet of finite thickness were derived by Donovan and Medcalf (14.16). Calculations were carried out for various parameters taken from InSb at room temperature. Rotation is similar to the results in Fig. 19. The loss curves in Fig. 20 show the high insertion loss due to surface reflections. Both rotation and loss are seen to increase with carrier concentration.

We expect to perform the experiments with carrier concentration equal to that of intrinsic material or higher in order to neglect the hole contribution whose mass is ten times as great as the electron effective mass. The interband Faraday effect which is oppositely directed to the free electron effect does not have any significant contribution (17) at the carrier concentrations and wavelengths being considered. Also the lattice vibrations (Reststrahlen bands) can be neglected at these wavelengths. The rotation is therefore dominated by conduction electrons.

Optical properties such as reflectivity and transmission have been measured in the infrared. Some of their results (22) are reproduced in Figures 21a and 21b for InSb. The

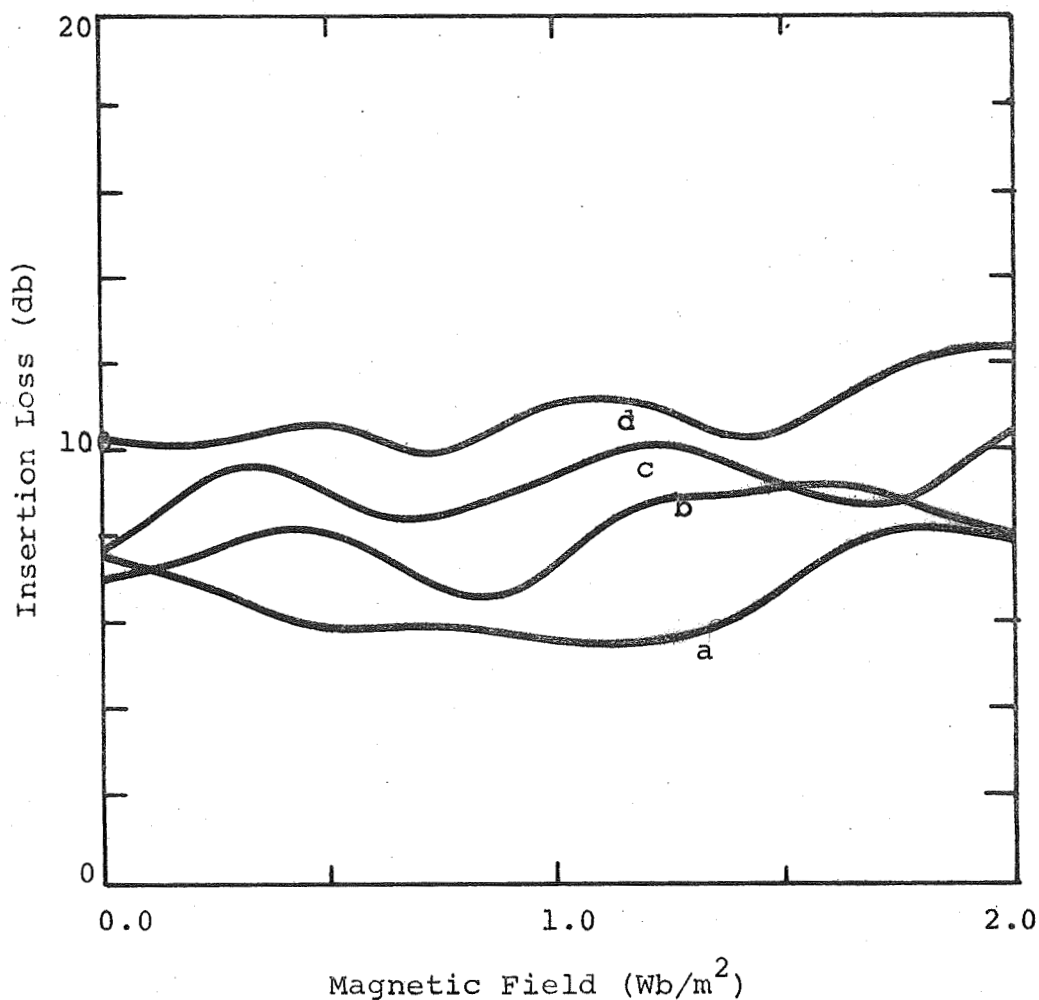


Fig. 20. Theoretical Insertion Loss Versus Magnetic Field

Computation Simulated for a sample of Indium Antimonide of various concentrations at room temperature

a.  $2.0 \times 10^{16} \text{ cm}^{-3}$   
 b.  $3.0 \times 10^{16} \text{ cm}^{-3}$

c.  $4.0 \times 10^{16} \text{ cm}^{-3}$   
 d.  $5.0 \times 10^{16} \text{ cm}^{-3}$

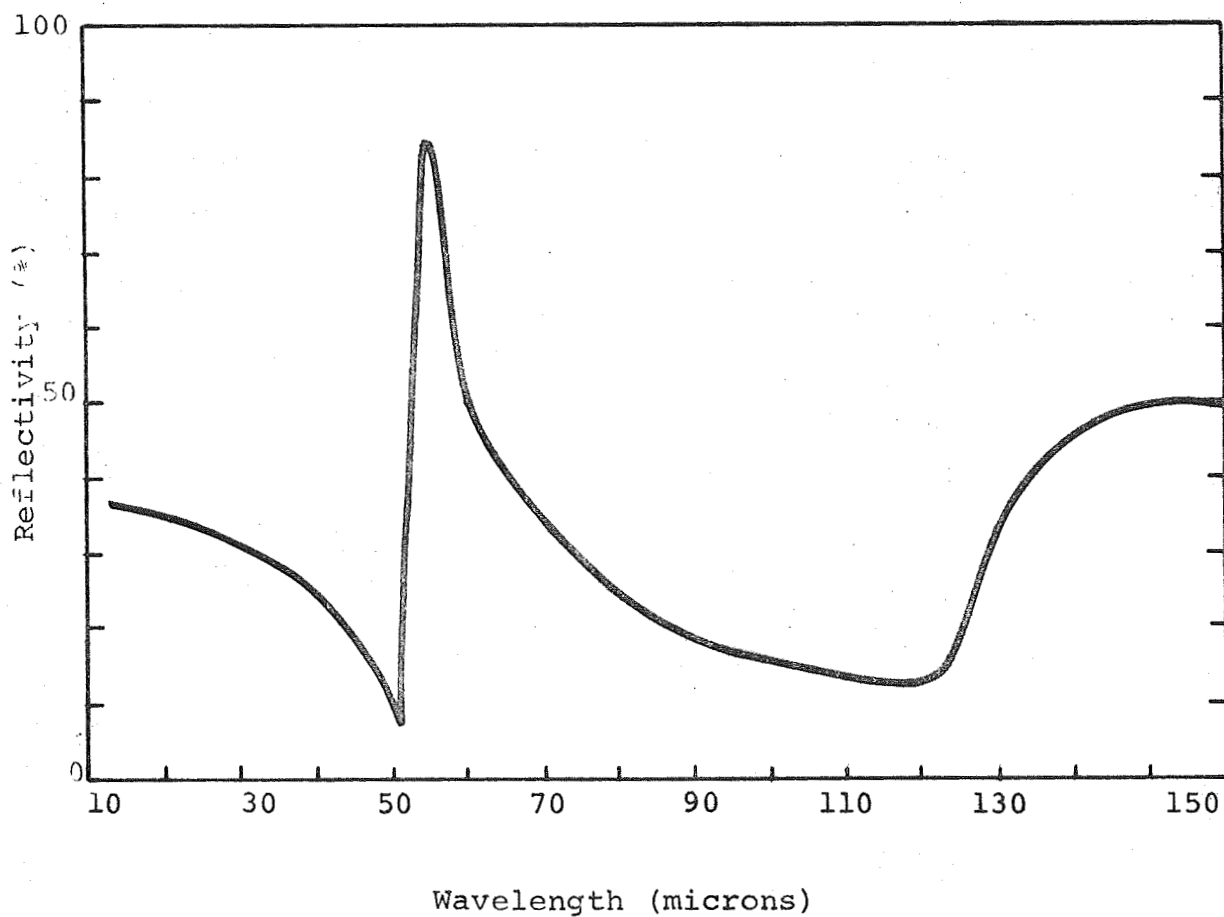


Fig. 21a. Reflectivity of Indium Antimonide Crystals

after H. Yoshinaga and R. Oetjen (18)

The Indium Antimonide sample has at 300°K  
the following electrical properties at 300°K

$$n = 2 \cdot 10^{16} \text{ cm}^{-3}$$

$\mu = 44000 \text{ cm}^2/\text{volt sec.}$   
and a thickness of 0.35mm

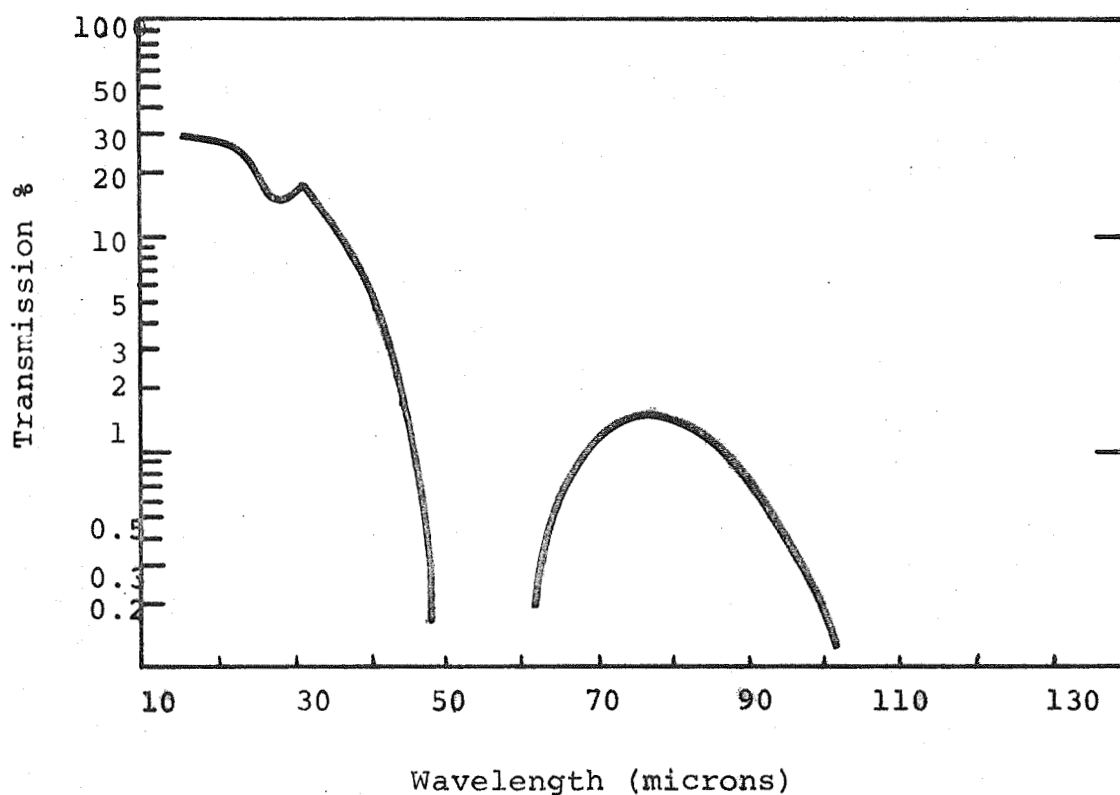


Fig. 21b. Transmission of Indium Antimonide Crystals  
after H. Yoshinaga and R. Oetjen (18)  
The Indium Antimonide sample of 0.35 mm  
thickness has the following electrical  
properties at 300°K

$$n = 2 \cdot 10^{16} \text{ cm}^{-2}$$

$$\mu = 44000 \text{ cm}^2/\text{volt sec.}$$

reflectivity by several workers (18), (19), (20), (21), (22) curve shows a sharp maximum at  $54.6\mu$  and the transmission shows a low transmission at the same wavelength due to lattice vibration in the crystal. A weak absorption at  $28.3\mu$  is due to the overtone of the lattice vibration. At  $27.9\mu$  the reflectivity is seen to be about 35% and the transmission about 25% for samples of 0.35mm thickness. Losses have been estimated theoretically and found to be of 6db for a sample 0.5mm thick in sample of similar electrical properties as the ones used in experiments by Yoshinaga and Oetjen. However this high loss can be avoided by using suitable impedance matching plates. The proposed scheme of the experiment for Faraday rotation measurement is presented in Figure 22.

### 3.3 Device Applications

#### 3.3.1 Isolator

Design calculations for an isolator using a data of InSb having at room temperature a concentration of about  $10^{16}$ - $10^{17}$  cm<sup>3</sup> and a mobility of  $80,000 \text{ cm}^2 \text{ v}^{-1} \text{ s}^{-1}$  and placed in a field of about 10 kG, have been carried out. The insertion losses for this transmission type isolator if no matching plates are used at the input and output is around 6db. By using suitable matching sections the isolator would then have less than one db forward transmission loss, making this device feasible. The device and experimental set up are shown in Figure 23.

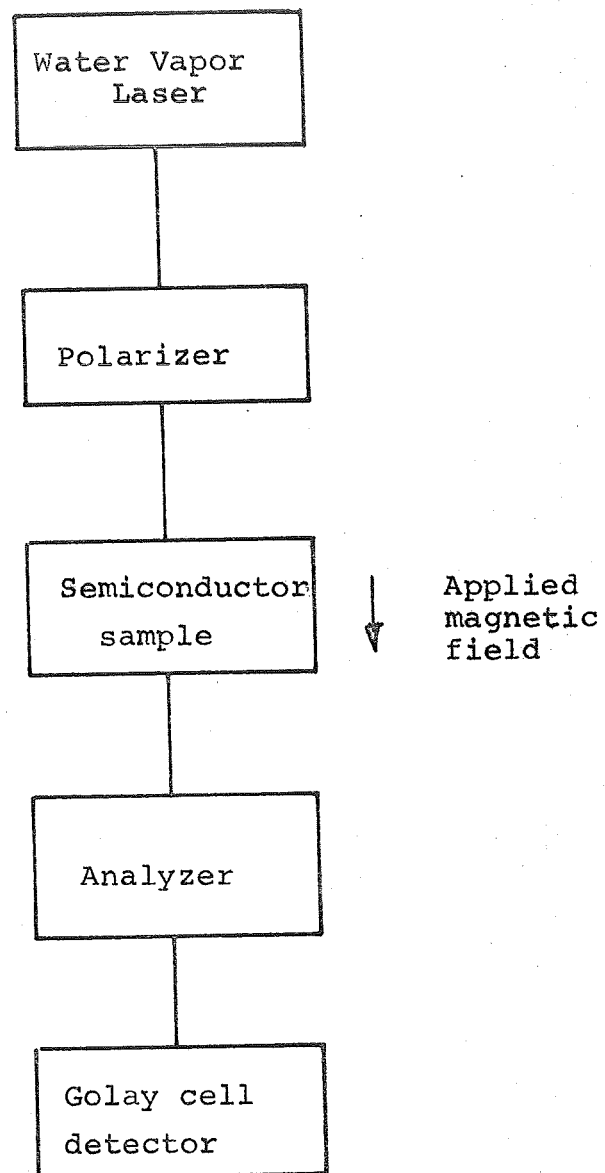


Fig. 22. Experimental Set up to Measure Faraday Rotation Angle

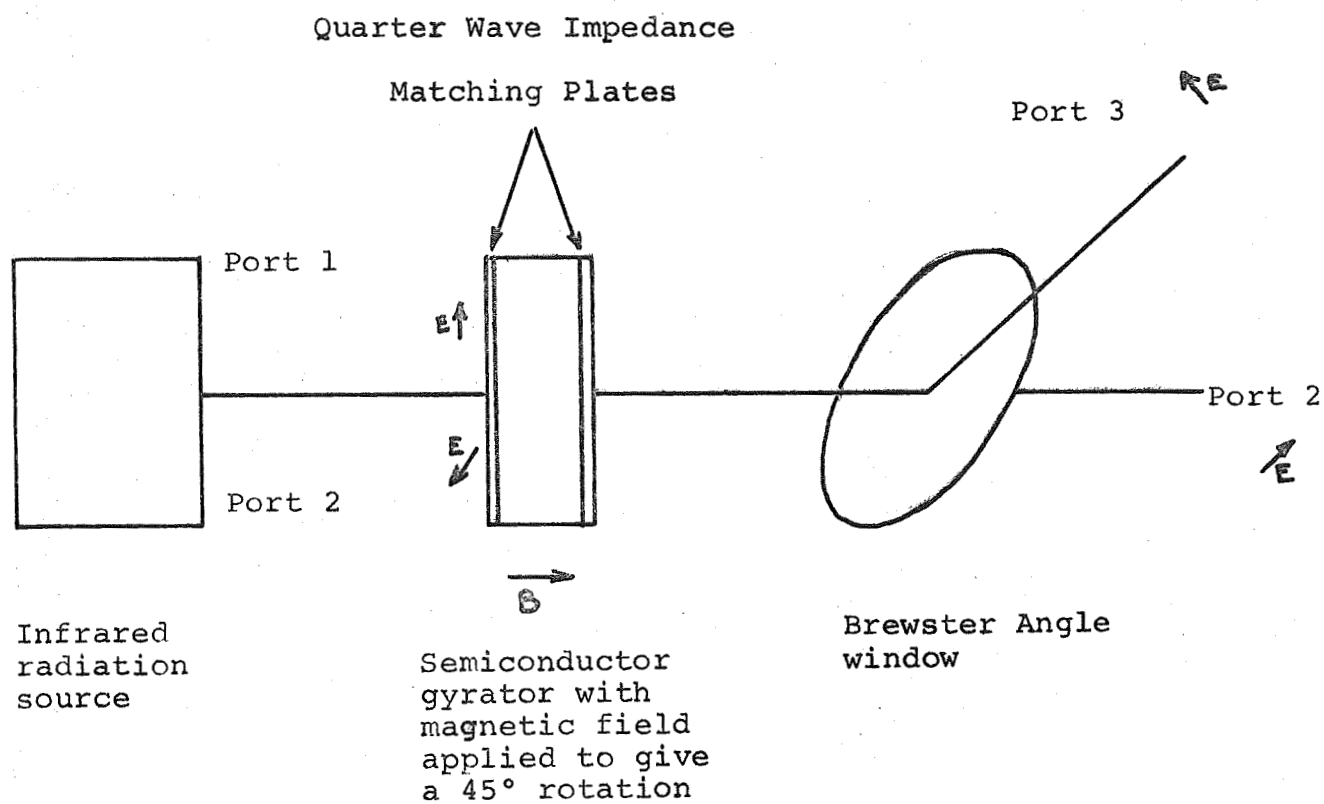


Fig. 23. Experimental set up to test the Proposed Faraday Rotation Isolator



### 3.3.2 Modulators

Free carriers modulators to be investigated will be designed to operate as reactance modulators as well as transmission devices which utilize the resistive free carrier modulation. Free carrier absorption in transmission devices has been investigated in Ge (23) and in high resistivity GaAs by several workers (24). Generation of free carriers can be achieved by several schemes, including:

- injection across a pn junction with current density of a few  $\text{A/cm}^2$  (25)
- photoabsorption of shorter wavelength light (26).

Figure 24 shows a proposed experimental set up for the infrared modulator constructed with a semiconductor rotator section.

### 3.4 Experimental Apparatus

#### 3.4.1 Design of Water Vapor Laser at 27.9 microns and at 118 microns

The geometrical design of the cavities resulted from the theoretical calculations of Li's paper (27) choosing for the Fresnel number  $N = \frac{a^2}{\lambda d} = 1.6$

$a$  = radius of the mirror

$d$  = cavity length

$\lambda$  = expected wavelength of operation

The laser glass tube cavity for 27.9 microns has an internal diameter of 2.5cm a length between mirrors of 3m and for 118

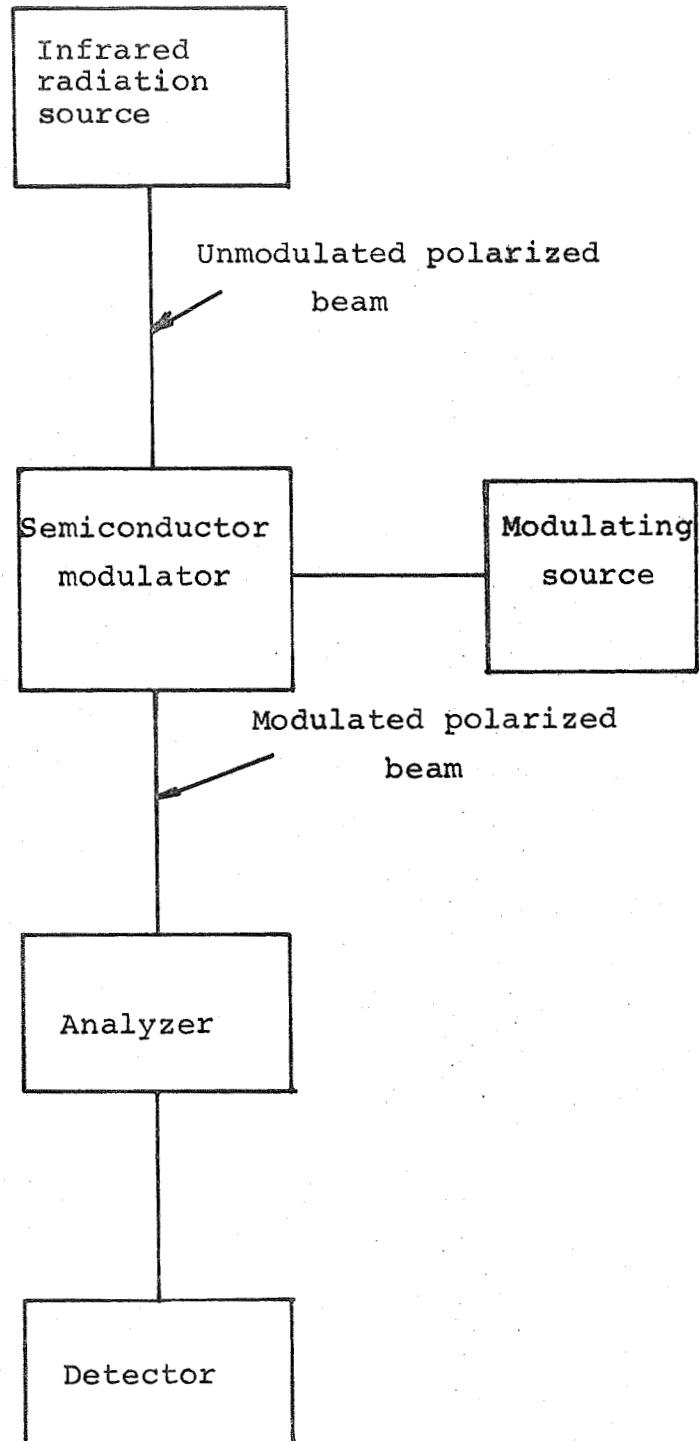


Fig. 24. Experiment set up to test the Proposed Faraday Rotation Modulator

microns, 5cm in diameter, 3.5m in length. Both are water cooled in order to increase the gain of the 27.9 $\mu$  and the 118 $\mu$  lines. The water cooled cathode and the anode are about 2.6m apart for 27.9 microns and 3.2m apart for 118 microns.

The resonator configuration sketched in Figure 25 is semi-confocal. The gold coated pyrex mirrors are 10cm in diameter two of them are flat, the other is spherically curved with a radius of 6m; their surface smoothness is within a 1/4 wave at 28 microns. The mirrors are mounted in supports that can be tilted in order to align optically the resonator. The two flat mirrors have an additional longitudinal motion controlled by differential micrometers.

A polarizer film has been placed inside the glass tube so as to have the output radiation linearly polarized in a known direction. The output window is made of high density polyethelene which has been found to be not too absorbing at 27.9 microns and also at 118 microns.

The laser output is detected by a Golay cell provided with a diamond window, the power output is expected to reach about 40mw, with both the 27.9 $\mu$  and 118 $\mu$  lasers.

This past report period has been spent on the designing and the operation of the gas laser and the calculations for the Faraday rotator designs. The difficulties encountered were due to:

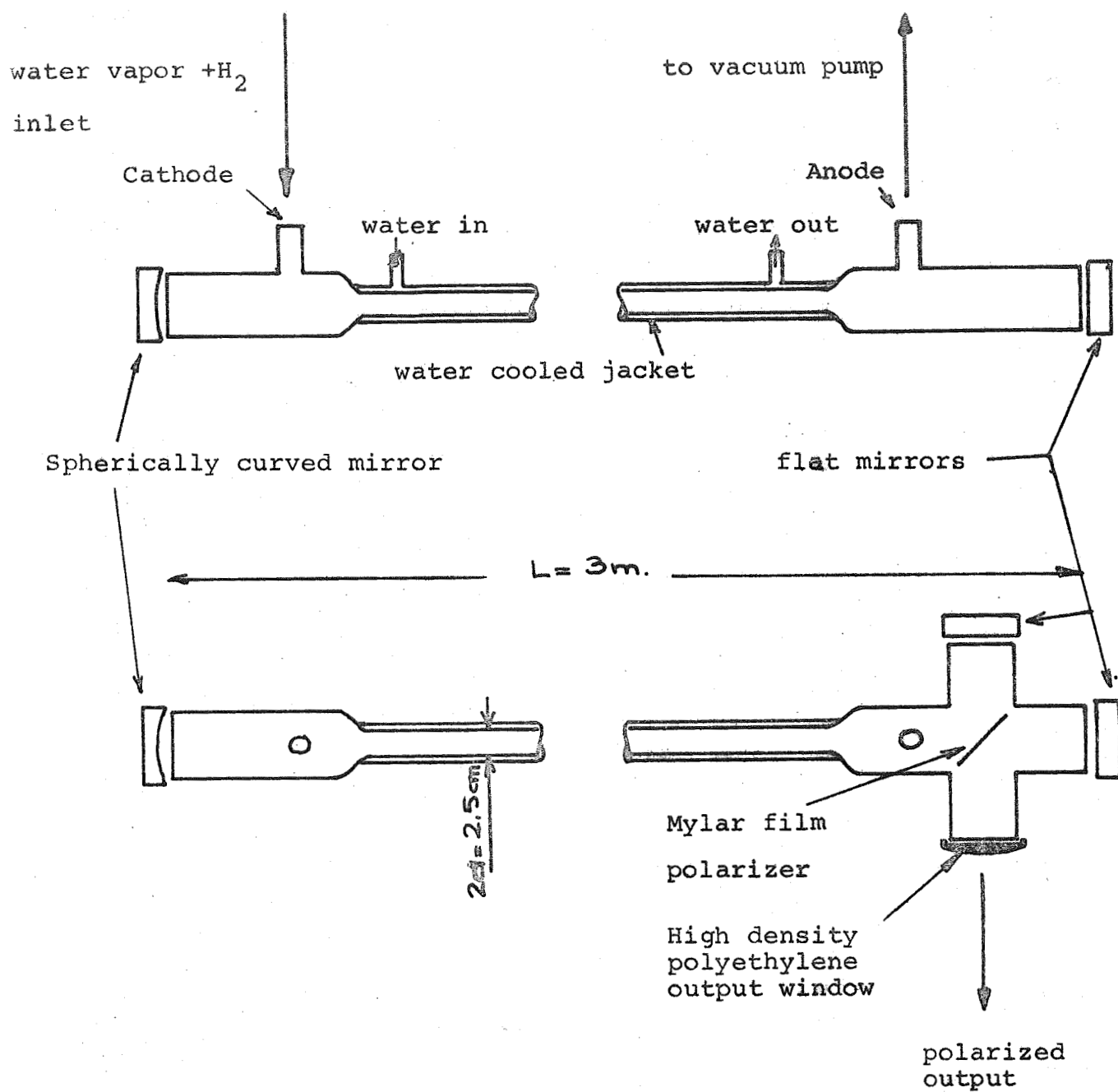


Fig. 25. Water Vapor Laser for the  
27.9 microns-line

1. The vacuum pump leaking some oil vapor into the system thereby contaminating the discharge with  $\text{CO}_2$ . The effect was a burned polarizer polyethelene film a few minutes after the discharge was ignited.
2. The mirror alignment procedure. Mirror alignment is somewhat critical at  $27.9\mu$  and the mirror mounts had to be rigid so that their position was the same with or without vacuum in the glass tube. The alignment method was performed with and without vacuum using an He-Ne laser. This procedure is thought to be very suitable for such a critical alignment.
3. The cathode and anode designs. The copper cathode had to be water cooled in order to avoid copper sputtering on the laser tube walls.

These problems have been solved and the laser should be expected to operate within the next few weeks.

### 3.5 Conclusions and Future Plans

Faraday rotation measurements will be performed with InSb at room temperature; materials like Ge, Si, GaAs are out of question, InAs could be a possibility if purer samples were available. This investigation will be followed by experiments on the Faraday Rotation isolators. The devices should be operating with fields around 10 kG and have forward loss of less than one db with matching plates. We expect to study these isolators at 27.9 and 118 microns.

Schemes for modulators will then be tried out. Modulator performances at this point are not known yet.

# APPENDIX A Reflection Coefficient for a Plane Boundary Between Solid State Plasma and Dielectric Material

Using cartesian coordinate shown in Fig. 4, a homogeneous solid state plasma occupies the space  $y > 0$  while a dielectric material occupies  $y < 0$ . The uniform magnetic field is parallel to the  $z$  axis.

By assuming a plane wave with harmonic time dependence  $\exp i\omega t$ , Maxwell's equations are given by

$$-j\omega\mu_0 \vec{H} = \nabla \times \vec{E} \quad (A-1)$$

$$-j\omega\epsilon_0 \vec{E} = \vec{K}^{-1} \nabla \times \vec{H} \quad (A-2)$$

Here the relative dielectric tensor of plasma has a form of

$$\vec{K} = \begin{vmatrix} K_{\perp} & -K_x & 0 \\ K_x & K_{\perp} & 0 \\ 0 & 0 & K_{11} \end{vmatrix}$$

where

$$K_{\perp} = \epsilon_{\ell} \left| 1 - \frac{j\omega_p^2 \tau (j\omega\tau + 1)}{\omega [(j\omega\tau + 1)^2 + \omega_C^2 \tau^2]} \right|$$

$$K_x = \epsilon_{\ell} \left| \frac{-j\omega_p^2 \omega_B \tau^2}{\omega [(j\omega\tau + 1)^2 + \omega_C^2 \tau^2]} \right|$$

and

$$K_{11} = \epsilon_0 \left| 1 - \frac{j\omega_p^2 \tau}{\omega(j\omega\tau + 1)} \right|$$

Then the inverse relative dielectric tensor of plasma is given by

$$\bar{K}^{-1} = \begin{vmatrix} A & -D & 0 \\ D & A & 0 \\ 0 & 0 & B \end{vmatrix}$$

where

$$A = \frac{K_{11}}{K^2 + K_x^2}, \quad D = \frac{K_y}{K^2 + K_x^2} \quad \text{and} \quad B = \frac{1}{K_{11}}$$

The wave equation derived from (A-1) and (A-2) are

$$\left( \frac{\partial^2}{\partial x^2} + \frac{\partial^2}{\partial y^2} + \frac{k_o^2}{A} \right) H_z = 0 \quad (\text{A-3})$$

$$\left( \frac{\partial^2}{\partial x^2} + \frac{\partial^2}{\partial y^2} + \frac{k_o^2}{B} \right) E_z = 0 \quad (\text{A-4})$$

where

$$k_o = \sqrt{\epsilon_o \mu_o} \quad \omega = \frac{2\pi}{\lambda}$$

The fact that  $H_z$  and  $E_z$  individually satisfy a wave equation means that any solution can be regarded as the linear combination of two partial solutions. Thus without any loss of generality attention can be restricted to the case of either  $H_z = 0$  or  $E_z = 0$ .

The solution for  $H_z = 0$ , however, is quite trivial one since the uniform magnetic field has no influence. Then consider the case of incident electric wave polarized in the plane of incidence. In free space,

$$H_{z, \text{ inc}}^0 = H_0 \exp [-ik \cos \theta \cdot y - ik \sin \theta \cdot x] \quad (\text{A-6})$$

where

$$k = \sqrt{\epsilon \mu_0} \omega$$

and the reflected wave is

$$H_{z, \text{ ref}}^0 = H_0 R \exp [ik \cos \theta \cdot y - ik \sin \theta \cdot x] \quad (\text{A-7})$$

where  $R$  is by definition a reflection coefficient. In plasma the transmitted wave must have a form

$$H_z = H_0 T f(y) \exp [-ik \sin \theta \cdot x] \quad (\text{A-8})$$

Where  $T$  is by definition a transmission coefficient. Since  $H_z$  is to satisfy a wave equation (A-4).

$$f(y) = \exp [-i \left( \frac{k_0^2}{A} - k^2 \sin^2 \theta \right)^{1/2} y]$$

Then

$$H_{z, \text{ trans}} = H_0 T \exp [-i \left( \frac{k_0^2}{A} - k^2 \sin^2 \theta \right)^{1/2} y - ik \sin \theta \cdot x] \quad (\text{A-9})$$

The boundary condition are that the tangential components of the fields in the plasma and in the dielectric media are to be continuous at  $y=0$ . The continuity of  $H_z$  at  $y=0$  gives



$$1+R = T . \quad (A-10)$$

$E_x$  components are evaluated from Eq. (A-2),

$$j\omega\epsilon E_{x, inc}^0 = -ik \cos\theta \cdot H_0 \exp[-ik\cos\theta \cdot y - ik\sin\theta \cdot x] \quad (A-11)$$

$$j\omega\epsilon E_{x, ref}^0 = -ik\cos\theta \cdot H_0 R \exp[ik\cos\theta \cdot y - ik\sin\theta \cdot x] , \quad (A-12)$$

and

$$j\omega\epsilon_0 E_{x, trans} = [-i(\frac{k_o^2}{A} - k^2 \sin^2\theta)^{\frac{1}{2}} A + (-ik\sin\theta) D] \cdot H_0 T \exp[-i(\frac{k_o^2}{A} - k^2 \sin^2\theta)^{\frac{1}{2}} y - ik\sin\theta \cdot x] . \quad (A-13)$$

Continuity of  $E_x$  at  $y=0$  then gives

$$\frac{\epsilon}{\epsilon_0} [(\frac{k_o^2}{k^2} \frac{1}{A} - \sin^2\theta)^{\frac{1}{2}} A + \sin\theta \cdot D] T = \cos\theta : (1-R) . \quad (A-14)$$

Using Eq. (A-10), the reflection coefficient  $R$  is

$$R = \frac{\cos\theta - \frac{\epsilon}{\epsilon_0} [(\frac{\epsilon_0}{\epsilon} \frac{1}{A} - \sin^2\theta)^{\frac{1}{2}} A + \sin\theta \cdot D]}{\cos\theta + \frac{\epsilon}{\epsilon_0} [(\frac{\epsilon_0}{\epsilon} \frac{1}{A} - \sin^2\theta)^{\frac{1}{2}} A + \sin\theta \cdot D]} , \quad (A-15)$$

and the transmission coefficient  $T$  is

$$T = 1+R = \frac{2\cos\theta}{\cos\theta + \frac{\epsilon}{\epsilon_0} [(\frac{\epsilon_0}{\epsilon} \frac{1}{A} - \sin^2\theta)^{\frac{1}{2}} A + \sin\theta \cdot D]} . \quad (A-16)$$

The skin depth  $\delta$  is given by the real part of propagation constant of the transmitted wave in y direction. Using Eq. (A-9), the skin depth  $\delta$  is given by

$$\delta = - \text{Imag} \left[ \frac{k_o^2}{A} - k^2 \sin^2 \theta \right]^{-\frac{1}{2}} \quad (\text{A-17})$$

## APPENDIX B DERIVATION OF FARADAY ROTATION AT INFRARED FREQUENCIES

Consider a uniform plane wave polarized along the x-axis and propagating along the magnetic field which is applied along the z-axis. Let the semiconductor slab which constitutes the solid state plasma zone to be infinite in length. This plasma is considered homogeneous, not lossy and the electron effective mass is isotropic. Applying Maxwell's equation:

$$\nabla \times \bar{E} = -j\omega\mu_0 \bar{H} \quad (B-1)$$

$$\nabla \times \bar{H} = \bar{J} + j\omega\epsilon_\ell \bar{E} = \left(1 + \frac{\bar{\sigma}}{j\omega\epsilon_\ell}\right) j\omega\epsilon_\ell \bar{E} \quad (B-2)$$

where

$$\bar{J} = \bar{\sigma} \bar{E}$$

$$\epsilon_\ell = \hat{\epsilon}_\ell \epsilon_0$$

and the tensor conductivity

$$\bar{\sigma} = \begin{vmatrix} \sigma_\perp & -\sigma_x & 0 \\ \sigma_x & \sigma_\perp & 0 \\ 0 & 0 & \sigma_{||} \end{vmatrix} \quad (B-3)$$

in which for an n-type semiconductor we have

$$\sigma_{||} = ne\mu/(1+j\omega\tau) \quad (B-4)$$

$$\sigma_\perp = \sigma_{||}/(1+A^2) \quad (B-5)$$

$$\sigma_x = \sigma_\perp A/(1+A^2) \quad (B-6)$$

$$A = \mu B/(1+j\omega\tau) \quad (B-7)$$

Solving the wave equation, and then separating into the x and y components we get

$$(\Gamma^2 - \omega^2 \mu_o \epsilon_\ell + j\omega \mu_o \sigma_\perp) E_x - j\omega \mu_o \sigma_x E_y = 0 \tag{B-8}$$

$$j\omega \mu_o \sigma_x E_x + (\Gamma^2 - \omega^2 \mu_o \epsilon_\ell + j\omega \mu_o \sigma_\perp) E_y = 0 \tag{B-9}$$

from which the dispersion relation can be written as

$$(\Gamma^2 - \omega^2 \mu_o \epsilon_\ell + j\omega \mu_o \sigma_\perp)^2 - (\omega \mu_o \sigma_x)^2 = 0 \tag{B-10}$$

Solving for  $\Gamma^2$  we obtain the expressions of the propagation constants for the right and left circularly polarized wave

$$\Gamma_+^2 = \omega^2 \mu_o \epsilon_\ell - j\omega \mu_o \sigma_\perp + \omega \mu_o \sigma_x \tag{B-11}$$

$$\Gamma_-^2 = \omega^2 \mu_o \epsilon_\ell - j\omega \mu_o \sigma_\perp - \omega \mu_o \sigma_x \tag{B-12}$$

The above expression show that the left-hand and the right-hand polarized waves propagate with different phase velocity under a magnetic field.

Upon replacing  $\sigma_\perp$  and  $\sigma_x$  one gets

$$\begin{aligned} \Gamma_\pm^2 &= -\omega^2 \epsilon_\ell \mu_o \left[ 1 - \frac{j\omega_p^2}{\omega (1 + j\tau(\omega \pm \omega_c))} \right] \\ &= (\alpha_\pm + j\beta_\pm)^2 \end{aligned} \tag{B-13}$$

where  $\alpha_\pm$  is the attenuation coefficient and,  
 $\beta_\pm$  the phase coefficient.

For infrared frequencies, with moderate magnetic fields and a sample of indium antimonide at room temperature some assumptions will be first justified and then applied to expression B-13 in order to simplify it.

Let the carrier concentration be

$$n = 3.0 \cdot 10^{16} \text{ cm}^{-3}$$

then the plasma frequency is given by

$$\omega_p^2 = \frac{ne^2}{m^* \epsilon_\ell} \quad (\text{B-14})$$

substitution of  $n$ ,  $e$ ,  $m^*$ ,  $\epsilon_\ell$  for the case considered leads to

$$\omega_p = 1.98 \cdot 10^{13} \text{ sec}^{-1}$$

The cyclotron resonance frequency is for  $B = 10^4 \text{ Gs}$

$$\omega_c = \frac{eB}{m^*} = 1.14 \cdot 10^{13} \text{ sec}^{-1} \quad (\text{B-15})$$

Radiation at  $27.9\mu$  has the corresponding frequency

$$\omega = 6.7 \cdot 10^{13} \text{ sec}^{-1}$$

The carrier lifetime for the sample considered is given by:

$$\tau = \frac{m^* \mu}{e} = 3.6 \cdot 10^{-13} \text{ sec} \quad (\text{B-16})$$

Therefore the following assumptions can be made:

- 1)  $\omega > \omega_B$
- 2)  $\omega \tau > 1$
- 3)  $\frac{\omega_p^2}{\omega^2} < 1$

(B-17)

Then the expression for the attenuation coefficient reduces to

$$\alpha_{\pm} = \frac{\omega_p^2}{2\omega^2 \tau} \sqrt{\epsilon_{\ell} \mu_0} \quad (\text{B-18})$$

and the expression for the phase coefficient becomes

$$\beta_{\pm} = 1 - \frac{\omega_p^2}{2\omega^2} \left(1 \pm \frac{\omega_C}{\omega}\right) \omega \sqrt{\epsilon_{\ell} \mu_0} \quad (\text{B-19})$$

This expression shows that the two circularly polarized waves will propagate with different phase velocities. This results in a rotation of the plane of polarization of the original linearly polarized wave as the wave propagates along the magnetic field in the solid state plasma.

The angle of this rotation is expressed by

$$\theta = \left( \frac{\beta_+ - \beta_-}{2} \right) d \quad (\text{B-20})$$

Replacing by B-19 one gets

$$\theta = \frac{\omega_p^2 \omega_C}{2\omega^2} \sqrt{\epsilon_{\ell} \mu_0} d$$

or upon substitution of  $\omega_p^2$  and  $\omega_B$  by B-14 and B-15 the expression becomes

$$\theta = \frac{ne^3 B d}{2\omega_m^2 \sqrt{\epsilon_{\ell}} c} \quad (\text{B-21})$$

### REFERENCES

1. Barber, N.F. and Crombie, D.D., "V.L.F. Reflections from the Ionosphere in the Presence of a Transverse Magnetic Field." Jour. Atmos. Terr. Phys., Vol. 16, pp. 37-45, 1959.
2. Waite, J.R., "Some Boundary Value Problems Involving Plasma Media", Jour. Res. Nat. Bur. Stand. 65B (Math. and Math. Phys.) No. 2, pp. 137-150, 1961.
3. Seaman, J.M., "Nonreciprocal Reflection of Microwave from a Solid State Magnetoplasma", M.S. thesis, University of Colorado, 1969.
4. Bremmer, H., "Terrestrial Radio Waves," Elsevier, Amsterdam, Netherlands, 1949.
5. Yabroff, I., "Reflection at a Sharply Bounded Ionosphere," Proc. IRE, 45, pp. 750-754, 1957.
6. Johler, J.R., and Walters, L., "On the Theory of Reflection of L.F. and V.L.F. Radio Waves from the Ionosphere," Jour. Res. Nat. Bur. Stand. 64D (Radio Prop.), pp. 269-285, 1960.
7. Crombie, D.D., "Reflection from a Sharply Bounded Ionosphere for V.L.F. Propagation Perpendicular to the Magnetic Meridian," Jour. Res. Nat. Bur. Stand. 65D (Radio Prop.) pp. 455-464, 1961.

8. Hilsum, C., "Some Key Features of III-V Components"  
Semiconductors and Semimetals, Vol. 2, pp. 9, 1966.
9. Wang, S., Solid State Electronics, McGraw-Hill, 1966.
10. Van der Pauw, L.J., "Method of Measuring Specific Resistivity and Hall Effect of Discs of Arbitrary Shape,"  
Phillips Research Report, Vol. 13, pp. 1-9, Feb. 1958.
11. Hogarth, C.A., "Materials Used in Semiconductor Devices,"  
John Wiley and Sons, Interscience Publishers, 1965.
12. McLeod, B.R., "Quasi-Optical and Waveguide Applications of Indium Antimonide," Ph.D. thesis, University of Colorado, Boulder, 1968.
13. Kuno, H.J., "Solid State Plasma Waveguides: Microwave Propagation and Faraday Effect," Ph.D. thesis, University of California, Los Angeles, 1966.
14. Hayes, R.E. and all, "The Application of Semiconductors to Quasi Optical and Waveguide Isolators for Use at Millimeter Wavelengths," NASA Report #NGR06-003-088, University of Colorado, July 1969.
15. Stephen, M.J. and Lidard A.B., "The Faraday Effect in Semiconductors," J, Phys. Chem. Solids 9, pp. 43-47, 1958.
16. Donovan, B. and Medcalf, T., "The Inclusion of Multiple Reflections in the Theory of the Faraday Effect in Semiconductors," Brit. J. Appl. Phys. 15, pp. 1139-1151, 1964.



17. Smith, S.D., Moss, T.S. and Taylor, K.W., "The Energy-dependence of Electron Mass in Indium Antimonide determined from Measurements of the Infrared Faraday Effect", J. Phys. Chem. Solids 11, pp. 131-139, 1959.
18. Yoshinaga, H. and Oetjen, R.A., "Optical Properties of Indium Antimonide in the Region from 20 to 200 Microns," Phys. Rev. 101, 2, pp. 526-531, Jan. 15, 1956.
19. Spitzer, W.G. and Fan, H.Y., "Infrared Absorption in Indium Antimonide," Phys. Rev. 99, pp. 1893-1894, 1955.
20. Kaiser, W. and Fan, H.Y., "Infrared Absorption of Indium Antimonide," Phys. Rev. 98, 4, pp. 966-968, May 15, 1955.
21. Blount, E. and all, "Infrared Absorption of Indium Antimonide," Phys. Rev. 101, 2, pp. 563-564, Jan. 15, 1956.
22. Sanderson, R.B., "Far Infrared Optical Properties of Indium Antimonide," J. Phys. Chem. Solids. 26, pp. 803-810, 1965.
23. Peters, D.W., "Infrared Modulator Utilizing Field Induced Free Carrier Absorption", Applied Optics, 6, 6, pp. 1033-1041, June 1967.
24. Walsh, T.E., "Gallium Arsenide Electro Optic Modulators," RCA Review, pp. 323-335, Sept. 1966.
25. McQuistan, R.B. and Schultz, J.W., "Modulation of Infrared by Free Carrier Absorption", J. Appl. Phys. 35, pp. 1243-1248, April 1964.

26. Grant, R.N., "Photoelectrically Induced Free Carrier Absorption", Applied Optics, 5, pp. 333, Feb. 1966.
27. Li, T., "Diffraction Loss and Selection of Modes in Maser Resonators with Circular Mirrors," Bell System. Tech. Journal, pp. 917-932, May 1965.